JOURNAL OF
CHEMICAL INFORMATION
AND MODELING

Subscriber access provided by UNIV OF NOTTINGHAM

Computational Biochemistry

Radical Stabilization Energies for Enzyme Engineering – Tackling the Substrate Scope of the Radical Enzyme QueE

Christian Suess, Floriane Martins, Anna Croft, and Christof M. Jäger

J. Chem. Inf. Model., **Just Accepted Manuscript** • DOI: 10.1021/acs.jcim.9b00017 • Publication Date (Web): 15 Nov 2019

Downloaded from pubs.acs.org on November 19, 2019

Just Accepted

"Just Accepted" manuscripts have been peer-reviewed and accepted for publication. They are posted online prior to technical editing, formatting for publication and author proofing. The American Chemical Society provides "Just Accepted" as a service to the research community to expedite the dissemination of scientific material as soon as possible after acceptance. "Just Accepted" manuscripts appear in full in PDF format accompanied by an HTML abstract. "Just Accepted" manuscripts have been fully peer reviewed, but should not be considered the official version of record. They are citable by the Digital Object Identifier (DOI®). "Just Accepted" is an optional service offered to authors. Therefore, the "Just Accepted" Web site may not include all articles that will be published in the journal. After a manuscript is technically edited and formatted, it will be removed from the "Just Accepted" Web site and published as an ASAP article. Note that technical editing may introduce minor changes to the manuscript text and/or graphics which could affect content, and all legal disclaimers and ethical guidelines that apply to the journal pertain. ACS cannot be held responsible for errors or consequences arising from the use of information contained in these "Just Accepted" manuscripts.

is published by the American Chemical Society. 1155 Sixteenth Street N.W.,
Washington, DC 20036

Published by American Chemical Society. Copyright © American Chemical Society.
However, no copyright claim is made to original U.S. Government works, or works
produced by employees of any Commonwealth realm Crown government in the course
of their duties.

Radical Stabilization Energies for Enzyme Engineering – Tackling the Substrate Scope of the Radical Enzyme QueE

Christian J. Suess†, Floriane L. Martins†, Anna K. Croft†, Christof M. Jäger†*

† The University of Nottingham, Department of Chemical and Environmental Engineering, University Park, Nottingham, NG7 2RD, United Kingdom.

ABSTRACT: Experimental assessment of catalytic reaction mechanisms and profiles of radical enzymes can be severely challenging due to the reactive nature of the intermediates, and sensitivity of cofactors such as iron sulfur clusters. Here we present an enzyme-directed computational methodology for the assessment of thermodynamic reaction profiles and screening for radical stabilization energies (RSEs) for the assessment of catalytic turnovers in radical enzymes. We have applied this new screening method to the radical SAM enzyme CPH_4 synthase (QueE), following a detailed molecular dynamics (MD) analysis that clarifies the role of both specific enzyme residues and bound Mg^{2+}, Ca^{2+} or Na^{+}. The MD simulations provided the basis for a statistical approach to sample different conformational outcomes. RSE calculation at the M06-2X/6-31+G* level of theory provided the most computationally cost-effective assessment of enzyme-based energies, facilitated by an initial triage using semi-empirical methods. The impact of intermolecular interactions on RSE was clearly established and application to the assessment of potential alternative substrates (focusing on radical clock type rearrangements) proposes a selection of carbon-substituted analogues that would react to afford cyclopropylcarbinyl radical intermediates, as candidates for catalytic turnover by QueE.

INTRODUCTION

Radical intermediates are extremely versatile for chemical functionalization and transformation reactions. Due to their high reactivity, radicals can facilitate these reactions with otherwise non-activated, unreactive substrates. However, this advantage comes at the cost that these highly reactive intermediates are particularly hard to control. This can lead to a multitude of possible unwanted side reactions and is one of the reasons why radical chemistry is predominantly found in industry for processes where either such side reactions are desirable or side reactions can be controlled or eliminated, for example in the downstream processing of crude oil (cracking) or in polymerization chemistry.

In nature, radical reactions play an important role in enzyme catalysis. The radical SAM enzyme superfamily is one group of enzymes that is capable of exploiting the potential of radical reactions in a very controlled way. These enzymes are able to initiate radical formation and direct their reaction by both preventing side reactions and facilitating the desired reaction simultaneously. This result of millions of years of evolution harnesses key similarities in catalytic mechanism, and yet results in a broad chemical reaction space (see reviews by Broderick et al.[1], Dowling et al.[2], and Jaeger and Croft[3] for a critical summary). Radical SAM enzymes catalyze reactions that include C-C bond formations,[4-6] decarboxylation reactions,[7] functional group migrations (1,2-shifts),[8-9] sulfur insertions,[10-13] methylations,[14-15] and more complex radical rearrangement mechanisms,[16-19] with these radical-mediated transformations involved in a multitude of biochemical synthesis routes that include compounds with antibiotic and antiviral activity. As such, it would be highly beneficial to gain access to and adapt these biotransformations for their use in industrial biotechnological applications, facilitating sustainable routes towards fine chemicals, pharmaceuticals, or bulk chemicals that would be highly challenging to synthesize by alternative methods.[3]

The key commonality for the catalysis of radical SAM enzymes is that they use S-adenosylmethione (SAM) either as cofactor or co-substrate. SAM is bound to a central Fe_4S_4 iron sulfur cluster responsible for initiating the redox reaction. The cluster is embedded via binding to cysteine residues of a conserved $CX_3CX\varphi C$ motif (with φ representing a conserved aromatic) and transfers an electron upon reduction to the SAM molecule which subsequently cleaves to afford the 5'-adenosyl radical (Ado•) and methionine (Met), which remains bound to the cluster. The Ado• radical represents the first reactive intermediate that then abstracts a hydrogen from a bound substrate to initiate catalysis.

Generally the control of radical intermediates in radical SAM enzymes is based on perfect positioning of the substrate towards the cluster bound SAM and the stabilization of the radicals. The argument is that more stable radicals are less likely to undergo unwanted side reactions, for example with the enzyme itself. However we recently showed with the example of the radical rearrangement in 7-carboxy-7-deazaguanine (CDG) synthase (QueE)[20] that this assumption is not always true. In the case of QueE, the unmodified substrate radical is so stable that the energy barrier for the subsequent radical rearrangement is too high for efficient catalysis, unless the radical is structurally or electronically perturbed.[21]

The reaction catalyzed by QueE represents a central step in queosine synthesis and facilitates the formation of the 7-deazapurine scaffold through a radical-mediated ring contraction.[22] Scheme 1 shows the radical rearrangement during the catalysis of QueE propagating through an azacycloproylcarbinyl intermediate followed by NH_2 elimination. This mechanism has been first described as one of two potential pathways by Drennan and coworkers,[20] and was confirmed computationally by Zhu and Liu[23] and us.[21] The rearrangement of CPH_4 proceeds after initial hydrogen abstraction from the C6 position through a cyclic azacyclopropylcarbinyl intermediate (3), before hydrogen re-abstraction from AdoH and deamination to form the final product (6). Intermediate 3 and its analogues also represent a class of structures known as radical clocks,[24] which undergo quick unimolecular rearrangements and have been described extensively by experiment and theory.[25-32]

We recently demonstrated that it is necessary to hold the substrate radical 2 in an energetically unfavorable configuration to overcome the rearrangement barrier for the ring conversion. This conformation is achieved by binding the substrate already in this conformation (which represents for the substrate a local energy minimum only slightly higher in energy than the unbound conformer) and hold this conformation after hydrogen abstraction through electrostatic fixation by a Mg^{2+} ion in the active site of the enzyme. Without this constraint, the radical would fall into a very stable, planar conformation and the energy barrier for the rearrangement would be too high for efficient reaction turnover. In other words, the substrate radical needs to be destabilized in order to facilitate the reaction.

This observation was also demonstrated by evaluating the stabilization of the radicals represented by radical stabilization energies (RSEs). By calculating the energy of a formal hydrogen transfer reaction (as described in the Experimental Section), RSEs inform on the reactivity of radicals in comparison to a given reference species. Thus, the higher the radical stabilization energy, the less energized and reactive the corresponding radicals are, also diminishing their role in unwanted side reactions. The concept of calculating RSEs has been used extensively for evaluating accurate absolute bond dissociation energies (BDEs) for a broad range of radicals including many systems related to peptides and enzyme catalysis.[33-40]

More recently Hioe and Zipse also demonstrated the usefulness of calculating radical stabilization energies for radical SAM enzymes.[40] They have calculated the thermodynamic reaction profiles for selected radical SAM enzymes on the basis of high-level RSE calculations in gas phase and demonstrated that enzymes using SAM as cofactor generally combine an initial exothermic hydrogen abstraction step with a subsequent endothermic step, while enzymes using SAM as co-substrate perform significantly exothermic H-abstraction reactions. What was not incorporated in this study was the effect on the radical stabilities and on the reaction profiles of binding to the enzyme and additional cofactors. As shown above, QueE is one such example where the intermolecular environment has a significant influence on these observables.

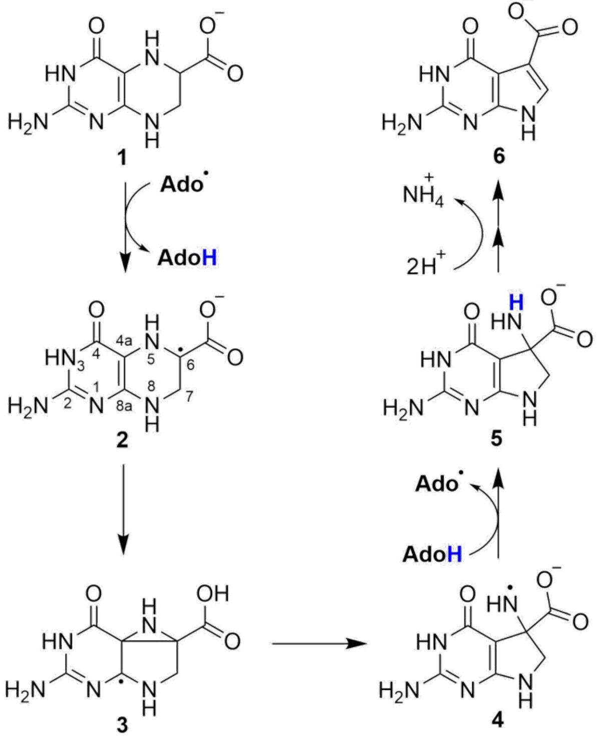

Scheme 1. Proposed ring contraction mechanism in the radical SAM enzyme QueE.

In this study, a combination of molecular dynamics (MD) simulations and RSE calculations is presented in order to investigate the effect of intermolecular binding on RSE estimation. It is demonstrated that a quick and affordable strategy can highlight if the enzyme environment facilitates significant changes to the reaction profile in comparison to the reaction assessed in gas phase or solution. Further, this information can subsequently be used to screen alternative substrate candidates for their potential for conversion, by comparing their reaction profiles to the native reaction. Potential enzyme mutation candidates can also be screened that may stabilize radical intermediates differently to the wild type enzyme. Thus, the combination of MD sampling and RSE calculations has the potential to be used as an initial tool for in silico enzyme design of radical SAM enzymes, bringing these enzymes one step closer to efficient biotechnological applications.

RESULTS AND DISCUSSION

MD SIMULATIONS

As previously indicated, QueE is found to facilitate catalysis only effectively in presence of Mg^{2+}.[20, 22] To investigate the effects on substrate binding and conformation in the presence of different ions in the enzyme, a series of molecular dynamics simulations have been carried out. Starting from the crystal structures of QueE[20] in complex with SAM, the substrate CPH_4 (1) and Na^+ (pdb code 4NJH) or Mg^{2+} (pdb code 4NJI) in the active site, the corresponding ions were either left unaltered, switched between the two structures, or substituted by Ca^{2+}. All simulations were run in 5 replicas and for at least 100 ns and maximal ~1 μs resulting in a total simulation time of approximately 8 μs.

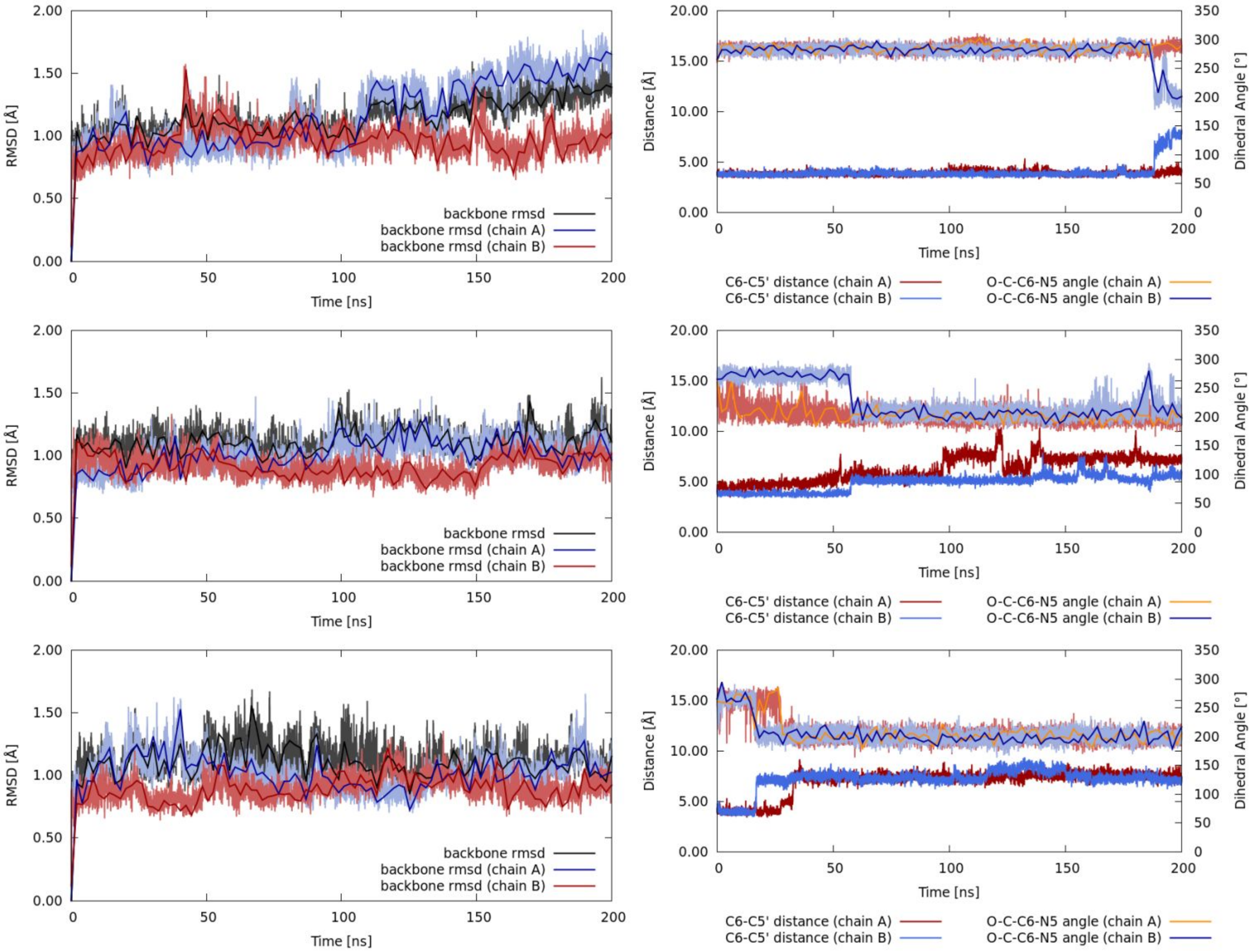

Figure 1. Analysis of 200 ns simulation time for CPH_4 bound to QueE in the presence of Mg^{2+} (top, MD-4NJI-Mg-2), Ca^{2+} (middle, MD-4NJI-Mg-1), and Na^+ (bottom, MD-4NJI-Na-1). The RMSD analysis (left) show high overall structural stability during simulation. The simulation time presented starts after 9 ns of restrained equilibration with the rmsd being calculated against the crystal structure configuration. The binding analysis of CPH_4 (right) depicts significant differences and changes for the binding position towards hydrogen abstraction (C6-C5' distance) and binding conformation (represented by the O-C-C6-H5 dihedral angle in CPH_4).

During the timeframe of all simulations, binding of SAM to the iron-sulfur cluster and the overall behavior of the dimeric enzyme showed high stability and low fluctuations. In a small number of simulations, conformational changes for SAM could be observed after several hundred nanoseconds, which was followed by the movement of a loop involved in SAM binding (see Figure S37 in the Supporting Information). Substrate unbinding, on the other hand, was observed in all cases after varying simulation time.

All simulations could reproducibly demonstrate significant differences for different ions in the active site. Based on the results of our previous study, which highlighted the need to bring the substrate into a bent conformation for optimal catalysis, the initial simulation analysis focused on analyzing this conformation and the positioning of the substrate for the initial hydrogen abstraction step.

Only simulations with Mg^{2+} in the active site kept the substrate in the bent conformation for significant simulation times, with the average retention time in the preferred conformation of 146 ns. The range covered binding of only 10 ns in one case and over 226 ns in other. Such long retention times were rarely seen for simulations containing Ca^{2+} and even less frequently for those containing Na^+, demonstrated by more flexible binding and much shorter retention times of the correct binding mode. The observed average retention times for these ions were 18 ns for Ca^{2+} (0-64 ns) and 2 ns (0-15 ns) for Na^+ based on the analysis of five replicate simulations for each of the systems containing the substrate and one of the ions Na^+, Mg^{2+}, Ca^{2+}, accounting for the sampling of 10 unbinding events for each system (see Table S26 in the Supporting Information for details). It should be noted that these retention times based on simulations starting from the bound conformers cannot be used to accurately calculate the binding affinities of the substrate to the enzymatic binding site. This would require a large set of very long free simulations sampling multiple binding and unbinding events and was not within the scope of this paper (see further discussion in the Supporting Information section 1.7).

Figure 1 depicts the essential binding analysis of substrate binding for three selected simulations over 200 ns each (more detailed analysis for all simulations can be found in Section 1.4 of the Supporting Information). All three simulations started from the crystal structure 4NJI with the substrate bound in the reactive conformation and the analysis started after careful and extensive restrained equilibration for 9 ns. The RMSD of all simulations remains low (Figure 1 left) and the SAM molecule remains bound to the iron sulfur cluster interacting with the unique iron through one carboxylate oxygen and the nitrogen of the methionine moiety. The carbon-carbon distance, essential for the hydrogen transfer between the C5' carbon of SAM and the C6 carbon of CPH_4, already depicts significant variation and differences. Without the need to calculate the transition state structure and energy for the hydrogen abstraction and on basis of structural sampling with SAM and not the cleaved Ado• radical, this C-C distance can already provide information on the relative likeliness for this initial hydrogen abstraction.

While for the Mg^{2+} simulation the substrate stays in adequate position for almost the entire 200 ns in both active sites of the dimeric enzyme, both substrates leave the correct position in the Ca^{2+} simulation within a few nanoseconds and even earlier during the simulation with Na^+. In most cases, leaving the initial position is directly coupled to changing into the more planar conformer of CPH_4 (also depicted in Figure 1). Only in some cases is the substrate seen leaving the pocket together with the tightly bound Mg^{2+} before the substrate changes its conformation. In contrast, in simulations with Ca^{2+} and Na^+ ions left the binding pocket without the substrate.

A more detailed look at substrate binding with different ions reveals further key differences (Figure 2). In all simulations, the substrate is fixed in the active site by hydrogen bonds between its carboxylate oxygens and the side chains of Arg27 and Thr90. Additional frequently found hydrogen bonds, common for all simulations, involve the side chains of residues Gln13 and Glu15 and the backbone of Gly14. The main variations between the simulations arise from the ion coordination within the active site.

Mg^{2+} coordinates throughout the whole simulation to one carboxylate and carbonyl oxygen, fixing the substrate in the bent conformation (Figure 2a). The ion is further coordinated by 4 water molecules but with no direct interaction observed with residues in the active site. Coordination to Asp50 and Thr51 is mediated through first shell water molecules. This is in slight disagreement with the crystal structure 4NJI, which suggests a direct coordination between Mg^{2+} and Thr51, but with unusual long interatomic distances of 2.7 and 2.9 Å (in the two binding sites respectively.[20] The two monomers in the crystal structure dimer also depict differences in the electron density in their active sites, which might be attributed to differing positions of water molecules or varying ion occupation over the average of the whole crystal (please refer to sction 1.5 of the Supporting Information for a more detailed comparison of simulation and crystallographic data). Interestingly, an additional simulation with the proposed intermediate **5** and Mg^{2+} in the active site (Figure 2d) resulted in a coordination chemistry resembling the crystal structure, with direct coordination between the ion and Thr51, 3 water molecules and the substrate. Further, the hydrogen bonding interaction between the carboxylate of the C-terminal Pro209 residue and the substrate, described in the crystal structure, is indicated as being much stronger in this intermediate-containing simulation. This contrasts with simulations containing bound substrate, where this interaction is loose and the C-terminus shows flexibility during the simulations.

Distinct from Mg^{2+}, Ca^{2+} coordinates the carbonyl oxygen of CPH_4 and Asp50 directly, while the contact to the carboxylate of the substrate is water-mediated (Figure 2b). The frequency of hydrogen bonding to Glu13 and Gln15 is also significantly reduced. This suggests additionally that, during the period where the substrate adopts the bent conformation, it is fixed less tightly in this conformation. This is certainly also the case in the very short time of correct binding observed with Na^+. The ion either leaves the pocket quite rapidly or is coordinated to Asp50 and the carboxylate of the substrate. Thus, the substrate flips rapidly into the planar conformation and also migrates from the optimal position for hydrogen abstraction.

In summary, clear differences for the binding of the substrate and the different ions in the active site are seen by MD simulation analysis. Mg^{2+} seems to place the substrate in much better position for abstraction and in the correct conformation, relative to what is seen for the other ions. However, the question as to what this effectively means for the radical rearrangement remains open.

RSE ASSESMENT

The calculation of radical stabilization energies (RSEs) relating to different substrates and intermediates can provide a clearer thermodynamic picture of radical reactions in radical SAM enzymes. These calculations alone, though, lack information about the influence of enzyme binding on the thermodynamic reaction profile. From the MD simulations and our previous work on a DFT model system[21] we already know that intermolecular interactions seem to have an important influence on the conformational space available for the reaction and thus on the stability of specific intermediates.

This study uses MD simulations as a sampling method for the system incorporating the bound substrate to then subsequently calculate the radical stabilization energies from multiple snapshots of these simulations. Firstly, this is applied without any further optimization of the structures from the simulations in order to get a rapid insight into changes in radical stabilization energies upon enzyme binding. Thus, these calculated values do not represent adiabatic radical stabilization energies, but vertical radical stabilization energies (vRSEs) neglecting geometrical relaxation after hydrogen abstraction.

Due to the lack of structural relaxation of the substrate and, more importantly, the radical, absolute vRSE values cannot be compared to accurate RSE values from high level DFT gas phase optimizations. However, when compared to the similar sampling in the gas phase it can provide direct information regarding how conformational restrictions in the active site might influence the stability of the intermediate generated during formation. In other words, it can signpost significant influences brought about by enzyme-induced binding and interactions.

In a second step, the protein environment is added to the calculations to look for further effects influencing radical stability. Additional residues can either explicitly be taken into account in the calculations or be represented by partial point charges. In that way, the impact of electrostatic effects in the active site in further influencing radical stability can be observed.

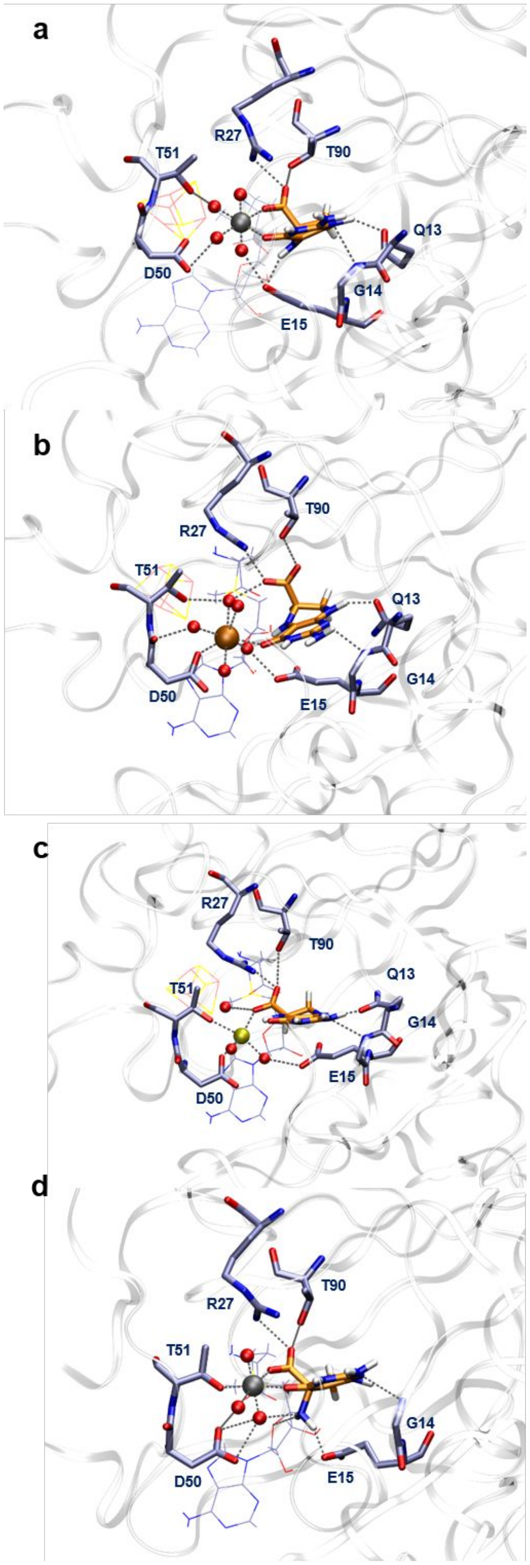

Figure 2. Substrate and ion binding in the active site of QueE. Snapshots taken from simulations with a) Mg^{2+} (MD-4NJI-Mg-1), b) Ca^{2+}(MD-4NJI-Ca-1), c) Na^{+}(MD-4NJI-Na-1). d) depicts the binding of intermediate **5** within the pocket in the presence of Mg^{2+} (MD-4NJK-Mg).

In a final step, the substrate and its radical form are optimized within a field of point charges representing the enzyme. This computationally more expensive QM/MM-type step confirms if the radical is able to substantially change its conformation once formed, and if this would have an effect of its stability and the energetic profile of the radical reaction.

An initial simulation where the substrate is bound correctly with Mg^{2+} was investigated. From this simulation, five thousand snapshots along a simulation time of 100 ns were extracted. For comparison, the same number of snapshots have been generated from a 500 ns simulation of the substrate in the gas phase. Subsequently, RSEs have been calculated for the C6 hydrogen abstracted radical (2) of the substrate for all snapshots on basis of the closed shell molecular mechanics geometries with a number of methods and basis sets.

Three exchange functionals (and standard Hartree-Fock calculations) and six basis sets have been considered and the results are shown in Table 1. Double and triple-ζ basis with polarisation and diffuse functions have been cross-analysed with functionals of varying degrees of sophistication. As expected, the Hartree-Fock (HF) calculations performed purely as standard implementations of HF are known to overestimate energies in protein systems and fail to describe dispersion correctly, making it an inappropriate method for thermochemical calculations. The Minnesota suite of functionals have been well received as suitable candidates for studying kinetics, thermochemistry and non-covalent interactions,[41] hence why two (M06-2X and M11) have been included in the preliminary calculations. Here the M06-2X functional was designed for these type of calculations, and the M11 has been presented as an improvement.[42] M06-2X was used for further calculations as it was a more dependable solution than M11, which had difficulty converging for this particular set of systems. All further calculations have also been corrected for dispersion by use of Grimme's D3 dispersion correction with correction values taken from literature.[43]

As the focus of this study depends more on relative shifts rather than absolute values, the choice of functional is not as significant as the choice of basis set. As long as a sensible choice is made, relative energy shifts are similar (see also Table S27 in the Supporting Information). In summary, calculations at the M06-2X/6-31+G* level of theory presented best-balanced cost-accuracy relation of all DFT methods tested and all following DFT results are presented using this approach.

Table 1. Averaged vRSE values for 5000 snapshots of 100ns of a MD simulation with Mg^{2+} and appropriately bound substrate (MD-4NJI-Mg-2, chainA) at different levels of theory. Energies are presented in kJ mol^{-1}.

	HF	B3LYP	M06-2X	M11
6-31G*	-237.3	-170.4	-146.5	-147.5
6-31+G*	-141.8	-37.7	-33.7	-40.6
6-31++G*	-238.2	-37.5	-33.5	-40.5
6-311+G*	-147.5	-34.2	-30.2	-30.3
6-311++G*	-147.2	-33.7	-29.8	-31.2
G3Large	-139.9	-25.9	-22.3	-20.9

RSE values have also been tested with semi-empirical (SE) methods to confirm their applicability for a quick RSE screening from MD data since the use of SE is significantly faster, with a speed up of around 1200-fold. A positive linear correlation between the calculated RSE values from both DFT (M06-2X/6-31+G*) and SE (PM6-D3) ($r2 = 0.86$Å) could be observed for the given example (see Figure S45 of the Supporting Information). This correlation allows the subsequent construction of a Gaussian distribution of the SE RSE's and then use of QM to calculate the RSEs of higher accuracy on a subset of selected frames near the Gaussian peak position (see Table S29 of the Supporting Information). This delivers RSE values of high accuracy at reduced calculation time.

The RSE values have then been calculated for the Mg^{2+}-bound substrate with and without optimization in the electrostatic field of the protein and have been compared to the initially calculated vertical RSE values. As can be seen from the data presented in Table 2, the vertical radical stabilization energies of the substrate radical bound correctly in the active site of QueE together with Mg^{2+} become significantly less negative by 34.0 kJ mol^{-1} in comparison to gas phase sampling only considering the substrate/radical itself in the conformation retrieved from the MD simulations directly. Thus, it can clearly be seen that the main contribution to the change in stability originates from the conformational change. Further, the standard deviation of the energies appears to be higher (SD ±20.2) for the bound conformations. This is also expected, as these radical conformations are not close to a stable conformational minimum and thus slight geometric changes represent larger energetic changes on the potential energy surface.

When the same procedure is repeated optimizing both the substrate and the radical in the electrostatic field of the protein, represented by atomic partial charges, the RSE values drop to more negative values. The shift in RSE upon enzyme binding even increases to 70.7 kJ mol^{-1} and while the standard deviation for the unconstrained gas phase system drops to a very low value of ±2.3, it remains high (±23.3) for the bound system. This once more indicates a radical in an uncomfortable conformation far from the preferred optimum and thus with large energy changes upon small structural changes.

Table 2. Radical stabilization energies from 100ns MD simulations of CPH6 in vacuum or bound to QueE with Mg^{2+} in the active site (MD-4NJI-Mg-2, chainA) at the M06-2X/6-31+G*(D3) level of theory. Energies presented in kJ mol^{-1}.

	RSE	SD	Shift[1]
Vacuum	-54.8	±13.1	0.0
Vacuum, optimized	-104.4	±2.3	0.0
Protein	-20.8	±20.2	34.0
Protein + point charges	-19.4	±15.6	35.5
Protein + pchg, opt	-33.7	±23.3	70.7

[1] The shift of the RSE values is calculated against the vacuum average (single point calculations or optimizations respectively).

When including the electrostatic field without further optimization (and comparison to the gas phase system) it can be seen that the electrostatic field seems to only have a small effect on radical stabilization for this example. Comparing the results after QM/MM optimization between DFT and SE calculations moreover shows that optimizations at the SE level are not reliable for calculating relative shifts of RSE values for constrained molecules (see Table S28 in the Supporting Information). Thus, the semi-empirical sampling can only be suggested for an initial sampling of MD trajectories as described before.

When comparing simulations of the substrate bound in the active site together with different cations, the consequences of the structural and dynamic differences seen in the MD simulations on the radical stability of the substrate in the enzyme are demonstrated very clearly. The average stabilization in cases where the substrate is bound in the correct conformation is shown to be significantly lower compared to unreactive binding of the substrate. As can be seen from Table 3 in a simulation where unbinding can be observed during the simulation with Ca^{2+} in the binding pocket, the vRSE value drops by over 25 kJ mol^{-1} from -33.9 (bound) to -59.1 kJ mol^{-1} (unbound).

Table 3. Vertical RSE values calculated from snapshots of MD simulations of QueE with substrate **1** and different cations at the M06-2X/6-31+G*(D3) level of theory. Single Point Energies are presented in kJ mol^{-1}.

Simulation ID[1]	Substrate position	Sampling time [ns]	Average RSE	SD
MD-4NJI-Mg-2	bound	0-200[1]	-20.8	20.2
MD-4NJI-Ca-1	bound	0-55[1]	-33.9	12.3
MD-4NJI-Ca-1	unbound	55-100[1]	-59.1	11.1
MD-4NJH-Ca-1	unbound	0-100[1]	-51.6	12.5
MD-4NJH-Na-1	unbound	0-100[1]	-51.2	11.5

[1] Simulation time presented starts counting after 9 ns of restrained simulation equilibration phase.

The effect of unbinding on the radical stability of the substrate (and thus on the thermodynamic reaction profile) can also be monitored in form of QM post-processing of the underlying MD simulation. In this way, changes of this central feature can be monitored in quasi-real (simulation) time without other analysis needed. Figure 3 demonstrates this for the Ca^{2+} simulation. The stability of the substrate radical shifts significantly after ~56 ns. Additional structural analyses confirm that this shift is correlated with movement of the substrate slightly out of the pocket, which changes the complexation to the cation and results in conformational change of the substrate. While the substrate is still anchored in the active site by the strong salt bridge between Arg27 and the substrate's carboxylate, it is not binding in a reactive fashion anymore. As demonstrated in the MD discussion above, this behavior is much more likely when Mg^{2+} is substituted by other cations in the active site.

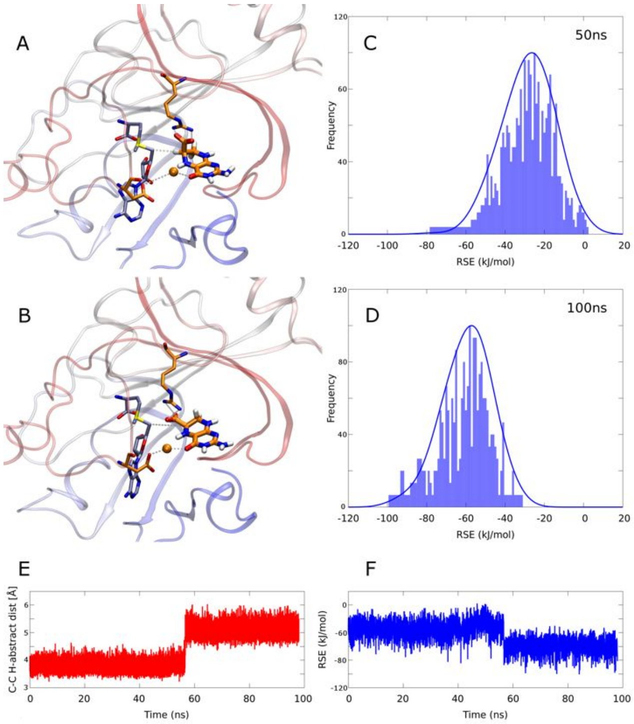

Figure 3. Representative snapshots of MD simulation of substrate CPH_4 (orange licorice) bound in QueE with Ca^{2+} (orange sphere) and SAM (licorice representation) in (a) active and (b) inactive (unbound) conformation. Distribution of M06-2X/6-31+G* vRSE values at over a time window of 1 ns after 50 and 100 ns simulation (MD-4NJI-Ca-1), including Gaussian fit to data (c, d) and plot of crucial H-abstraction C-C distance (e) and vRSE values (f) over 100 ns simulation.

POTENTIAL SUBSTRATE SCOPE OF QueE

In the view of the possibility to apply the method to calculate vRSE values for radical enzymatic reactions in the context of protein engineering, a set of alternative substrates have been tested for their potential to be converted through a similar reaction mechanism to the natural substrate QueE. A set of structures were selected that are also able to react via an analogous radical rearrangement through either an azacyclopropylcarbinyl radical or their carbon- and sulfur-substituted analogues. The structures were chosen to represent different substitutions next to the radical center that either stabilize or destabilize the radical by electron pushing or pulling effects, or might influence substrate binding through the presence or absence of functional groups necessary for hydrogen bonding. The selected structures are listed in Figure 4.

The results were evaluated taking into account the following selection criteria for potential alternative substrates of QueE: 1) the correct positioning of the substrate carbon involved in the necessary first hydrogen abstraction step between the **Ado•** radical and the potential substrate to initiate the radical rearrangement; 2) the corresponding docking score as an indicator for substrate affinity to the pocket (This score is also compared to the lowest docking score of the corresponding substrate to see whether alternative binding conformations are more likely); 3) the radical stabilization energy of the substrate in order to evaluate if a high rearrangement barrier is to be expected; 4) the RSE after optimization in the electrostatic field. This last assessment adds information about the likelihood of a substrate to be bound in a preferred conformation for catalysis, but where the radical would undergo quick relaxation to form a stable inactive radical intermediate.

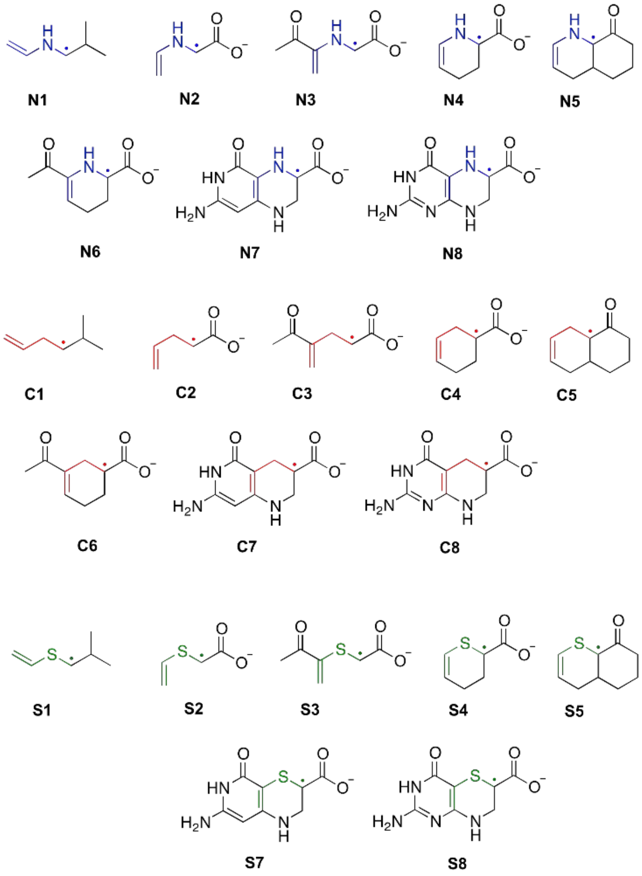

Figure 4. Alternative substrate radicals considered for docking and RSE studies.

All these four criteria do not only give valuable information about whether a potential substrate might be a good candidate for catalysis, but also indicate potential ways to improve the candidacy by signposting additional mutations within the enzyme's active site. The full docking results are presented in the Table S30-31 in the Supporting Information and the most interesting results are briefly discussed below.

From the docking calculations, the three conformers of each molecule with the best docking score have been taken for further RSE analysis. Additional docking studies without including the Mg^{2+} ion in the active site were also performed to investigate if some substrates might be suitable for transformation without the support of the ion.

Table 4. Calculated radical stabilization energies and rearrangement barriers (Ea) for QueE. Energies presented in kJ mol^{-1}.

	RSE		Ea	
	M06-2X^{c}	G3B3	M06-2X^{c}	G3B3
N1	-60.8	-57.6	99.5	
N2	-73.9	-73.8	105.6	102.1
N3	-87.2	-82.2	132.0	123.9
N4	-98.5		117.8	
N5	-137.1		174.1	
N6	-107.0	-95.5	138.1	130.3
N7	-104.6		143.4	
N8	-94.0		143.3	
C1	-26.4	-23.6	43.2	
C2	-90.3	-88.9	82.4	83.8
C3	-50.2	-49.1	39.5	38.8
C4	-54.0		50.2	
C5	-78.0		93.1	
C6	-47.2	-38.9	65.5	68.3
C7	-41.4		95.6	
C8	-47.8		101.8	
S1	-47.3		65.2	
S2	-52.1	-56.0	69.9	69.7
S3	-53.5	-58.7	71.1	70.5
S7	-64.7		136.3	
S8	-71.4		138.7	

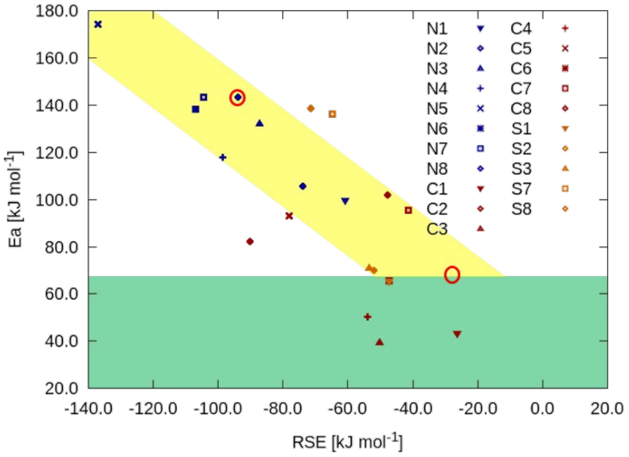

Figure 5. Calculated radical stabilization energies and rearrangement barriers (Ea) for QueE. The trend for the correlation between the activation barriers and RSE values values is highlighted in yellow. The green area represents rearrangement barriers approximately suitable for catalysis (rearrangement barrier <75 kJ mol^{-1} which represents the upper limit of the activation barrier for the initial hydrogen abstraction observed in enzymatic catalysis).[44-45] The red circles highlight the values for the natural substrate CPH$_4$ in gas phase and in the model system from our previous study.[21]

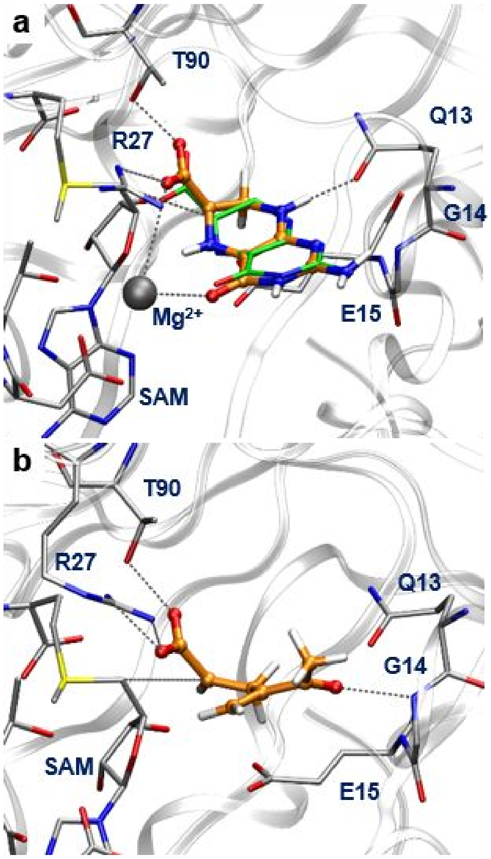

Figure 6. a) natural substrate radical **2** (orange ball and stick representation) after docking and geometry optimization in the active site of QueE superimposed with the crystal structure of CPH$_4$ (**1,** green licorice). b) alternative **ligand C3** after docking and geometry optimization in QueE without Mg^{2+}.

Applying this protocol to the natural substrate CPH$_4$ (**N8**) (see Table 5) delivered reasonable docking poses with and without Mg^{2+} in the active site. Subsequent RSE calculations including QM/MM geometry optimisations could confirm an increase in radical stabilization but the structures did not relax to a very stable planar conformation, making the rearrangement in principle possible.Across the complete dataset, substrates docked in preferential position and conformation often drop into a more preferable and less reactive radical conformation with high radical stabilization upon optimization. This indicates that these substrates are unlikely to undergo a catalytic rearrangement and that additional mutations of active site residues might be necessary to further maintain reactive conformations. Further, the observation that the single point calculations including the point charge (PC) field, but neglecting further optimizations, differ much more significantly from single point calculations without the PC field (compared to the results from vRSE single point calculations based on MD simulations) indicates that equilibration after docking is necessary for an adequate interpretation and reliable results, either through MD or geometry optimizing the structures.

Unsurprisingly, substrates without carbonyl or carboxylic functional groups cannot be attached strongly to residues in the active site (in particular Arg27) and thus result in very low docking scores and variable docking orientations (Table S31 in the Supporting Information). Thus, substrates **C1**, **C2**, **C4**, and C5, for example, show relative low RSE values, but do not bind strongly enough or in the correct position for catalysis and are very unlikely to act as alternative substrates.

For structures able to facilitate supporting anchoring by Arg27, on the other hand, catalytic turnover might be possible (see ligands **C3**, **C6**, **C7**, and **C8** in Table 5) with improved positioning and even without Mg^{2+} support in some cases. Figure 6b depicts ligand **C3** docked and subsequently optimized in its radical form in the pocket of QueE without Mg^{2+} demonstrating adequate positioning and radical stabilization for enzymatic turnover. In general, the cyclopropylcarbinyl precursors, that do not need to overcome a similar high transition barrier to the aza-cyclopropylcarbinyl analogues, might function better without Mg^{2+} due to better positioning. Also, ligand **N3** (which includes the anchoring carbonyl but lacks the ring structure of the natural substrate) might undergo turnover without Mg^{2+} as its radical does not need to be fixed in a tightly bended conformation.

Table 5. Selected RSE values with and without QM/MM geometry optimization in the point charge (PC) environment, based on docked structures of alternative substrates from Figure 4. XPscore denotes the extra precision Glide docking score, and the C6-C5' distance indicates the crucial distance for the initial hydrogen abstraction reaction in the docked structure. Full results can be found in Table S30.

				RSE [kJ mol^{-1}]			
Ligand (docking rank)	With / without Mg^{2+}	XPscore (kJ/mol)	C6-C5' distance (Å)	SP (vRSE)	SP with PC	Opt with PC	RMSD
C3 (1)	Mg^{2+}	-26.6	4.57	-9.4	-6.7	-51.9	1.04
C3 (3)	Mg^{2+}	-27.6	4.47	-11.3	-5.7	-56.1	0.89
C3 (1)	-	-14.3	4.00	-4.9	4.6	-20.7	0.41
C3 (1) MD 150 ns	Mg^{2+}	-26.6	4.59 ±0.27	-18.4 ±9.9	-9.9 ±10.5	-37.5 ± 15.3	
C6 (1)	Mg^{2+}	-28.3	4.60	-4.7	7.6	-86.4	1.14
C6 (2)	-	-21.4	3.92	-18.3	-14.8	-46.9	0.21
C7 (1)	-	-17.5	3.65	-8.1	-2.5	-19.0	0.33
C8 (2)	Mg^{2+}	-33.7	5.21	-5.9	-8.1	-65.5	0.68
C8 (1)	-	-15.5	3.75	-8.1	-2.9	-17.3	0.29
N3 (1)	Mg^{2+}	-28.6	5.42	-20.2	-17.9	-26.2	1.19
N3 (3)	Mg^{2+}	-28.8	3.91	-14.4	-12.1	-112.2	0.85
N3 (2)	-	-12.9	4.27	-21.4	-11.2	-48.8	0.53
N8 (1)	Mg^{2+}	-28.1	3.80	-43.9	-46.9	-77.1	0.17
N8 (2)	Mg^{2+}	-32.2	5.56	-14.4	-12.6	-33.4	0.17
N8 (1)	-	-30.6	3.76	-38.9	-38.5	-84.9	0.19
N8 (2)	-	-21.8	5.01	-42.1	-43.5	-59.9	0.22

On the other hand, structures that are placed well for initial hydrogen abstraction but where significant stabilization occurs upon optimization effectively might act as inhibitors. Although they show the principle potential for rearrangement, they are trapped in a low energy minimum after hydrogen abstraction and thus are inhibited from further turnover. Examples showing this behavior for all conformers analyzed are ligands **C4** and **N4** (see Table S30-31 in the Supporting Information for details).

To further prove the potential suitability of alternative substrate **C3** we have conducted another set of MD simulations based on the docked structures with and without Mg^{2+} and followed up by RSE assessments. The simulations, performed in triplicate, showed that the initial assumption of good binding without Mg^{2+} resulted in relatively rapid unbinding of the alternative substrate in all three simulations. With Mg^{2+} in the active site, the simulations showed stable binding for at least 70 ns in one case and for the full simulation time of 150 ns in the other two cases. Subsequent RSE analysis of 300 snapshots (shown in Table 5) of one of the simulations confirmed the observations from the docking simulations demonstrating suitable binding and RSE stabilization for turnover. Therefore, the MD simulations added a crucial binding equilibration assessment, not available by simple docking assessments and should be added to any workflow applied to selected hit structures.

In summary, this first combined docking and RSE assessment gives new insights into how the radical enzyme QueE controls the central catalytic radical rearrangement. The protocol developed here offers a new and suitable approach to assess the thermodynamic reaction profile of natural and alternative substrates in radical SAM enzymes. Excitingly, it has good potential to serve as a pre-screening tool for alternative substrates in radical enzymes, as a first step towards enzyme engineering in this underexploited domain.

CONCLUSION

Radical stabilization plays an important role in the enzymatic catalysis of radical SAM enzymes. Often the way intermediate radicals are stabilized or destabilized within the active site determines the rate determining steps of the catalysis of these enzymes. In cases where the reaction mechanism is known, evaluating the thermodynamic reaction profiles for these enzymes offers an affordable gateway into computational predictions of substrate scope and initial steps into reengineering substrate scope, turnover, or promiscuity of these enzymes.

In this study on QueE we show that the combination of MD simulations and the evaluation of radical stabilities delivers deeper understanding in how the enzyme controls enzymatic turnover and what the crucial role of the central Mg^{2+} ion is, namely that tight control of the reactive radical conformation and stability is only supported by Mg^{2+} ions but not by other cations. This is represented by tighter binding of the substrate in the reactive Michaelis complex conformations as demonstrated by longer retention times in this conformation and the significant lowering of the radical stabilization of the substrate radical in this conformation that correlates with a lowering of the transition barrier for the radical rearrangement.

Applying a combination of substrate docking and radical stabilization assessment on a set of alternative substrates delivered detailed information about potential alternative substrates and inhibitors. We could confirm that only ligands that show significant lower stabilization in their preferred conformation, or substrates that can be stabilized in a less preferred conformation in the enzyme, are likely to act as alternative substrates. Cyclopropylcarbinyl precursors were shown to be more likely to undergo turnover than heteroatom substituted analogues, based on their smaller radical stabilization and lower rearrangement barriers. Also, anchoring to Arg27 by a functional group of the ligands (preferably by carboxylates) is necessary to bring the ligands in optimal position (for initial hydrogen abstraction) and stabilize reactive conformations for potential turnover.

These results show that there is significant potential in the presented methodology to be used as a screening approach for enzyme engineering of radical SAM enzymes, other radical enzymes/processes, and more broadly for enzymes that proceed *via* other highly reactive intermediates (*e.g.* those proceeding through reactive cationic intermediates). Screening thermodynamic reaction profiles is easier and quicker to perform than more costly transition state searches for multistep reactions, like the reaction presented here, and the use of intermediate energies in such reactive systems is supported by Hammond's postulate, provided similar systems are compared. Further, the use of this type of screening is particularly relevant in these cases, as the reactivity of the intermediate often means that its generation is also the rate determining step in the enzyme process.

The next step for this methodology is to screen for mutations in the active site, either supporting turnover for alternative substrates or altering turnover for the natural substrate, in this case CPH_4. Such alterations may improve reactivity, or provide leverage for greater selectivity for a mixture of similar substrates, alongside providing a greater insight into the contributions of both individual and groups of residues on the mechanism. Having a rapid screen at hand to look at mutants will serve as the entry point for the computational design of radical SAM enzymes and other processes proceeding through reactive species, facilitating the development of reactions with non-natural substrates for the generation of novel, bioactive compounds.

In this spirit, we propose a general computational screening methodology for alternative substrates for radical SAM enzymes and mutants of radical SAM enzymes as outlined in Figure 7. The methodology starts with identifying features of the natural enzyme-substrate complex. Subsequent docking screens and MD equilibrations of hit structures are followed by further alternative mutant screens to find potential alternative substrates and enzyme mutants capable to react with these substrates. A more detailed technical workflow can also be found in Section 4 of the Supporting Information and is freely available in form of a Jupyter Notebook application.

As mentioned before, the central RSE evaluation within the workflow serves as a rapid evaluation of the thermodynamic energy difference between a highly reactive intermediate and the substrate that correlates to the kinetic reaction barrier when the system follows Hammond's postulate. Therefore, it is necessary to know if a relationship between the thermodynamic reaction data and the bottleneck of the catalytic reaction exists.

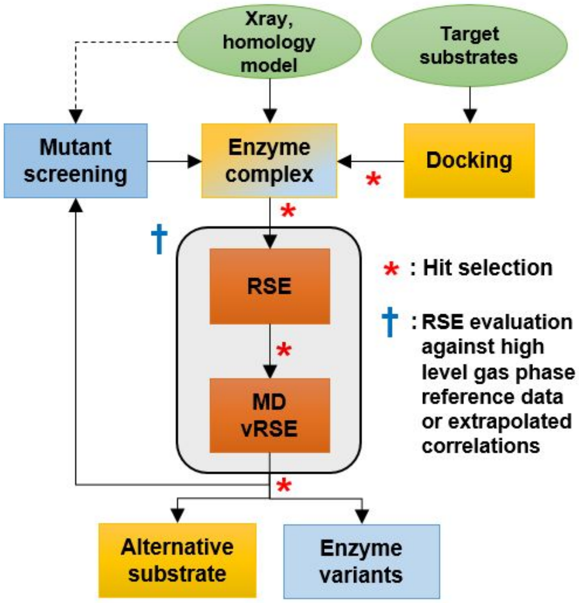

Figure 7. Proposed computational workflow for screening for alternative rSAM enzyme substrates and alternative mutants based on the rapid assessment of radical stabilization energies.

We also propose that this screening workflow is transferable to a wide variety of enzyme engineering applications if the above-mentioned requirement is satisfied and the chemical and structural change between the substrate and the high energy intermediate is small (as given for a wide range of hydrogen or proton transfer and other reactions). The latter is necessary to ensure that MD sampling of the enzyme-substrate complex is sufficient to be able to calculate the thermodynamic reaction properties as described. Otherwise, it would be necessary to perform the MD sampling with the substrate and the intermediate, which would double the computational effort.

When transferring the workflow to other examples only the central RSE assessment needs to be replaced by the corresponding thermodynamic reaction profile of the target reaction. This should make this approach easily adaptable to other protein and catalyst engineering applications.

EXPERIMENTAL SECTION

Additional information and more detailed methods are provided in the Supporting Information. All simulation coordinates, input and important analysis files (in particular relevant MD interatomic distance analysis) are also available online on the figshare repository (DOI: https://doi.org/10.6084/ m9.figshare.c. 4290332.v2). Additional analysis scripts (perl) and cpptraj input files are also presented there. Computational workflows developed for the calculation of vRSE values from MD data on GitHub (https://github.com/ChrisSuess/RSE-Calc).

Molecular Dynamics Simulations

All molecular-dynamics simulations were performed using the GPU implementation[46-48] of the Amber16[49] molecular dynamics package. The force field parameters for SAM are based on electrostatic reparametrized force field parameters from Saez and Vöhringer-Martinez[50] as described and tested previously.[51] The parameters for the 4Fe4S cluster are based on a recent parametrisation of biological relevant iron-sulfur clusters by Carvalho and Swart.[52] These parameters showed good structural identity of the clusters as shown in the MD analysis in Section 1.4 of the Supporting Information. For embedding the cluster into the enzyme the sulfur charges of connected cysteine residues have been adapted to the charges from the model compounds used for the parametrisation and the charge of the unique iron atom have been adjusted to remain the total charge of +1 for the reduced cluster. The parameters for the divalent cations were taken from Li et al.,[53] those for monovalent ions to neutralise the total charge of the system from Horinek et. al.[54]

Electrostatic point charges for SAM were reparametrised following the restrained electrostatic potential (RESP) fitting procedure by Kollman *et al.*[55] and are based on multiconfigurational fitting of three different conformers. The structures for RESP fitting were taken from the crystal structures of butirosin biosynthetic enzyme,[56] BtrN (pdb entry 4M7T), tRNA-wybutosine synthesising enzyme, TYW2 (pdb entry 3A25),[57] and 7-carboxy-7-deazaguanine synthase, QueE (pdb entry 4NJI),[20] and have been picked in order to represent different bent and stretched SAM conformations. After geometry optimisation at the B3LYP[58-60]/6-31+G(d)[61-62] level of theory including diffuse functions[63] and applying the polarisable continuum model (PCM)[64] as implicit solvation model with Gaussian09[65] two sets of charges were derived. The first set was prepared following the standard RESP procedure at the HF/6-31G(d) level, and a second set was generated based on PCM-B3LYP/cc-PVTZ[62] calculations in implicit solvent with a dielectric constant of 4.335, that is suitable for representing the electrostatic environment in a protein more closely. The parameters of the substrate CPH4 and the substrate intermediate (2K8) have been parametrised on the basis of the general amber force field (GAFF)[66] using the same RESP fitting procedure as described above.

The interaction of SAM and the cluster was treated by electrostatic interactions only. No restraints have been applied to the cluster, the substrate, or SAM apart from the simulation equilibration. Only in some rare cases the unique (non-bonded) iron of the cluster inverted when no SAM molecule was bound. This might be due to the fact that the parametrisation included very low angle force constants and was based on fully bound clusters without unique Fe atoms.

All simulations have been performed in explicit solvent, using the SPC/E[67] water model and the Amber force field FF12SB for all standard amino acids within the enzyme structures. The protonation state of titratable amino acids has been determined using the software of the H++ server.[68]

The simulations were conducted at a temperature of 300 K using periodic boundary conditions. Electrostatic long range interactions were treated with the Particle Mesh Ewald (PME)[69] and a 12 Å cut-off for nonbonding interactions was applied. The temperature in all simulations was controlled by coupling the system with the Langevin thermostat with collision frequency set to 2 ps^{-1}. An integration time step of 2 fs was used and the SHAKE algorithm was employed to constrain bonds involving hydrogen atoms during the MD simulation.

All simulations were treated with a restrained equilibration strategy prior to data collection. Firstly, all structures were minimized in four minimization steps of combined steepest descent and conjugate gradient minimisation for 1000 steps each following a partial release of positional restraints with a force constant of 50 kcal mol^{-1}. Restraints have been applied for minimizations 1-4 as follows: 1) Protein, 4Fe4S clusters, central ion, SAM, ligands, crystal water; 2) protein, 4Fe4S clusters, central ion, SAM, ligands; 3) protein, 4Fe4S clusters, central ion, SAM; 4) 4Fe4S clusters, central ion, SAM. This was followed by a heat up phase of the system were the protein, SAM, the 4Fe4S clusters, and the central ions were restrained with a force constant of 20 kcal mol^{-1} for 100 ps of simulation. Finally, the systems were further equilibrated at constant pressure (NPT) molecular dynamics at one atmosphere using a Langevin directed dynamics for pressure control with restraints of 20 kcal mol^{-1} on 4Fe4S clusters, central ion, and SAM for another 900 ps, and with weaker restraints of 10 kcal mol^{-1} on the same residues for another 8 ns. The final production runs for the simulations were performed for at least 100 ns and over 1500 ns in maximum. The simulations have been repeated several times starting from the same starting coordinates, but applying different initial velocities to the atoms.

All MD simulations are based on the following crystal structures:

4NJI: QueE from Burkholderia multivorans in complex with AdoMet (SAM) and 6-carboxy-5,6,7,8-tetrahydropterin (CPH6) and Mg^{2+}; 4NJH: QueE from Burkholderia multivorans in complex with AdoMet (SAM) and 6-carboxy-5,6,7,8-tetrahydropterin (CPH6) and Na^{+}; 4NJG: QueE from Burkholderia multivorans in complex with AdoMet (SAM) and 6-carboxypterin (CP6); 4NJK: QueE from Burkholderia multivorans in complex with AdoMet (SAM), 7-carboxy-7-deazaguanine (CDG), and Mg^{2+}.

Simulations performed using pdb 4NJI include the substrate (CPH6) in its reactive conformation, simulations based on pdb 4NJH in its non-reactive conformation (with Na^{+}). A comparative simulation with the substrate analogue CP6 has been performed using pdb 4NJG. The simulation with intermediate **4** is based on pdb 4NJK (including the product CDG in the crystal structure).The complete list of all simulations included into this paper can be found in Table S1 of the Supporting Information.

DFT and RSE calculations

All accurate RSE calculations for alternative substrates were performed analogue to our previous publication on QueE[21] and as outlined for reactions in radical SAM enzymes by Hioe and Zipse.[40] Their calculations represent a formal hydrogen abstraction between closed shell precursors (e.g. the substrate CPH4) and a reference radical, such as CH_3• for carbon centered radicals and NH_2• for nitrogen centered radicals, as given in Equations 1 and 2.

$$CH_3^{\bullet} + \text{H-R} \longrightarrow CH_4 + R^{\bullet} \qquad (1)$$

$$NH_2^{\bullet} + \text{H-R} \longrightarrow NH_3 + R^{\bullet} \qquad (2)$$

Based on these processes, the resulting reaction enthalpies can be calculated as defined in Equation 3:

$$\text{RSE}(R^{\bullet}) = H_{298}(R^{\bullet}) + H_{298}(CH_4) - H_{298}(\text{R-H}) - H_{298}(CH_3^{\bullet}) \qquad (3)$$

These energy values are also referred to as radical stabilization energies (RSEs), which technically represent the relative stability of the radicals against a given reference, and can be referenced against accurate bond dissociation energies (BDEs) through accurate experimental values of the reference systems. The calculated RSE values were corrected with unscaled zero-point energies on the level of their geometry optimization. RSE energies were then calculated applying thermal corrections to enthalpies at 298.15 K at the level of their geometry optimization. All stationary points have been characterized by frequency calculations.

For the calculation of the vertical radical stabilization energy (vRSE) values snapshots from the trajectories of the dynamic simulations were analyzed with single point energy calculations, at both a semi-empirical (SE) and density functional level of theory (DFT). All semi-empirical calculations reported were carried out using MOPAC[70] a semi-empirical quantum chemistry package based on Dewar and Thiel's NDDO approximation[71] with the PM6-D3 method which uses Grimme's D3 dispersion corrections for correlation.[43] All DFT calculations use the quantum chemistry package Q-Chem[72] at an M062X/6-31+G(d) level of theory. Grimme's D3 dispersion corrections are applied where: s6 = 1.0, sr,6 = 1.619 and s8 = 0.0.

All accurate RSE calculations for alternative substrates were performed analogue to our previous publication on QueE[21] and as previously outlined for reactions in radical SAM enzymes by Hioe and Zipse.[40] All geometry optimizations and frequency calculations of the open-shell systems and their restricted counterparts were performed at the UB3LYP[58-60]/6-31+G(d) and the UBMK[73]/6-31+G(2df,p) levels, including diffuse functions.[63] Stationary points were confirmed by calculating their normal vibrations. Higher level single point calculations were performed on all B3LYP geometries at the M06-2X[74]/6-311++G(3df,3p) level and with the more accurate G3B3[75] methodology wherever affordable. All relative energies were corrected with unscaled zero-point energies on the level of their geometry optimization. RSE energies were then calculated applying thermal corrections to enthalpies at 298.15 K at the level of their geometry optimization. All optimized geometries can be found on the figshare repository.

Docking calculations

The prepared set of substrates was docked into the receptor QueE using a combined standard precision (SP) extra precision (XP) protocol with Glide[76-77] as described in detail in Section 3.1 of the Supporting Information. Following an exhaustive sampling search to predict orientation, conformation and binding position of a structure inside the rigid receptor pocket by Glide SP, the best conformers of each substrate were selected and docked with Glide XP to retain more accurate results. The OPLS3 force field[78] was used for the docking calculations and no constraints were applied.

ASSOCIATED CONTENT

Detailed description of the simulation, DFT, and docking setups, complete results of the docking and vRSE calculations, further graphical analysis, Cartesian coordinates, and force field parameters used are given in the Supporting Information. This material is available free of charge via the Internet at http://pubs.acs.org.

AUTHOR INFORMATION

Corresponding Author

* christof.jaeger@nottingham.ac.uk

Author Contributions

The manuscript was written through contributions of all authors. All authors have given approval to the final version of the manuscript.

Funding Sources

EU FP7 Marie Curie Actions - People, Co-funding of Regional, National and International Programmes (COFUND) under Grant Agreement no PCOFUND-GA-2012-600181. European Cooperation in Science and Technology (COST) network CM1201. EPSRC Ref EP/P011993/1 Cloud-based methods to predict the druggability of protein-protein interactions: applications to cancer and antimicrobial resistance.

ACKNOWLEDGMENT

AKC and CMJ would like to acknowledge support from the European Cooperation in Science and Technology (COST) network CM1201. CMJ acknowledges funding through the Nottingham Advanced Research Fellowship and EU FP7 Marie Curie Actions - People, Co-funding of Regional, National and International Programmes (COFUND) under Grant Agreement no PCOFUND-GA-2012-600181. We also gratefully acknowledge support and access to the University of Nottingham High Performance Computing Facility.

ABBREVIATIONS

BDEs, bond dissociation energies; DFT, density functional theory; MD, molecular dynamics; pdb, protein database; QM/MM, quantum mechanics/molecular mechanics; QueE, 7-carboxy-7-deazaguanine synthase ; RMSD, root mean square deviation; RSEs, radical stabilisation energies; SAM, S-adenosylmethione.

REFERENCES

(1) Broderick, J. B.; Duffus, B. R.; Duschene, K. S.; Shepard, E. M., Radical S-adenosylmethionine enzymes. *Chem. Rev.* **2014,** *114*, 4229-4317.

(2) Dowling, D. P.; Vey, J. L.; Croft, A. K.; Drennan, C. L., Structural diversity in the AdoMet radical enzyme superfamily. *Biochim. Biophys. Acta Proteins Proteom.* **2012,** *1824* (11), 1178-1195.

(3) Jäger, C. M.; Croft, A. K., Anaerobic Radical Enzymes for Biotechnology. *ChemBioEng Reviews* **2018,** *5* (3), 143-162.

(4) Magnusson, O. T.; Toyama, H.; Saeki, M.; Schwarzenbacher, R.; Klinman, J. P., The Structure of a Biosynthetic Intermediate of Pyrroloquinoline Quinone (PQQ) and Elucidation of the Final Step of PQQ Biosynthesis. *J. Am. Chem. Soc.* **2004,** *126* (17), 5342-5343.

(5) Barr, I.; Latham, J. A.; Iavarone, A. T.; Chantarojsiri, T.; Hwang, J. D.; Klinman, J. P., Demonstration That the Radical S-Adenosylmethionine (SAM) Enzyme PqqE Catalyzes de Novo Carbon-Carbon Cross-linking within a Peptide Substrate PqqA in the Presence of the Peptide Chaperone PqqD. *J. Biol. Chem.* **2016,** *291* (17), 8877-8884.

(6) Cooper, L. E.; Fedoseyenko, D.; Abdelwahed, S. H.; Kim, S.-H.; Dairi, T.; Begley, T. P., In Vitro Reconstitution of the Radical S-Adenosylmethionine Enzyme MqnC Involved in the Biosynthesis of Futalosine-Derived Menaquinone. *Biochemistry* **2013,** *52* (27), 4592-4594.

(7) Bruender, N. A.; Bandarian, V., The radical S-adenosyl-l-methionine enzyme MftC catalyzes an oxidative decarboxylation of the C-terminus of the MftA peptide. *Biochemistry* **2016,** *55* (20), 2813-2816.

(8) Lepore, B. W.; Ruzicka, F. J.; Frey, P. A.; Ringe, D., The x-ray crystal structure of lysine-2,3-aminomutase from Clostridium subterminale. *Proc. Natl. Acad. Sci. U.S.A.* **2005,** *102* (39), 13819-13824.

(9) Ruzicka, F. J.; Frey, P. A., Glutamate 2,3-aminomutase: a new member of the radical SAM superfamily of enzymes. *Biochim. Biophys. Acta* **2007,** *1774* (2), 286-296.

(10) Lanz, N. D.; Lee, K.-H.; Horstmann, A. K.; Pandelia, M.-E.; Cicchillo, R. M.; Krebs, C.; Booker, S. J., Characterization of Lipoyl Synthase from Mycobacterium tuberculosis. *Biochemistry* **2016,** *55* (9), 1372-1383.

(11) Cicchillo, R. M.; Iwig, D. F.; Jones, A. D.; Nesbitt, N. M.; Baleanu-Gogonea, C.; Souder, M. G.; Tu, L.; Booker, S. J., Lipoyl Synthase Requires Two Equivalents of S-Adenosyl-l-methionine To Synthesize One Equivalent of Lipoic Acid. *Biochemistry* **2004,** *43* (21), 6378-6386.

(12) Berkovitch, F.; Nicolet, Y.; Wan, J. T.; Jarrett, J. T.; Drennan, C. L., Crystal Structure of Biotin Synthase, an S-Adenosylmethionine-Dependent Radical Enzyme. *Science* **2004,** *303* (5654), 76-79.

(13) Fugate, C. J.; Jarrett, J. T., Biotin synthase: Insights into radical-mediated carbon–sulfur bond formation. *Biochim. Biophys. Acta Proteins Proteom.* **2012,** *1824* (11), 1213-1222.

(14) Boal, A. K.; Grove, T. L.; McLaughlin, M. I.; Yennawar, N. H.; Booker, S. J.; Rosenzweig, A. C., Structural Basis for Methyl Transfer by a Radical SAM Enzyme. *Science* **2011,** *332* (6033), 1089-1092.

(15) Layer, G.; Moser, J.; Heinz, D. W.; Jahn, D.; Schubert, W.-D., Crystal structure of coproporphyrinogen III oxidase reveals cofactor geometry of Radical SAM enzymes. *EMBO J.* **2003,** *22* (23), 6214-6224.

(16) Hänzelmann, P.; Schindelin, H., Crystal structure of the S-adenosylmethionine-dependent enzyme MoaA and its implications for molybdenum cofactor deficiency in humans. *Proc. Natl. Acad. Sci. U.S.A.* **2004,** *101* (35), 12870-12875.

(17) Chatterjee, A.; Li, Y.; Zhang, Y.; Grove, T. L.; Lee, M.; Krebs, C.; Booker, S. J.; Begley, T. P.; Ealick, S. E., Reconstitution of ThiC in thiamine pyrimidine biosynthesis expands the radical SAM superfamily. *Nat. Chem. Biol.* **2008,** *4* (12), 758-765.

(18) Sicoli, G.; Mouesca, J.-M.; Zeppieri, L.; Amara, P.; Martin, L.; Barra, A. L.; Fontecilla-Camps, J. C.; Gambarelli, S.; Nicolet, Y., Fine-tuning of a radical-based reaction by radical S-adenosyl-L-methionine tryptophan lyase. *Science* **2016,** *351* (6279), 1320-1323.

(19) Yu, Y.; Duan, L.; Zhang, Q.; Liao, R.; Ding, Y.; Pan, H.; Wendt-Pienkowski, E.; Tang, G.; Shen, B.; Liu, W., Nosiheptide Biosynthesis Featuring a Unique Indole Side Ring Formation on the Characteristic Thiopeptide Framework. *ACS Chem. Biol.* **2009,** *4* (10), 855-864.

(20) Dowling, D. P.; Bruender, N. A.; Young, A. P.; McCarty, R. M.; Bandarian, V.; Drennan, C. L., Radical SAM enzyme QueE defines a new minimal core fold and metal-dependent mechanism. *Nat. Chem. Biol.* **2014,** *10* (2), 106-112.

(21) Jäger, C. M.; Croft, A. K., Radical Reaction Control in the AdoMet Radical Enzyme CDG Synthase (QueE): Consolidate, Destabilize, Accelerate. *Chem. Eur. J.* **2017,** *23* (4), 953-962.

(22) Bandarian, V.; Drennan, C. L., Radical-mediated ring contraction in the biosynthesis of 7-deazapurines. *Curr. Opin. Struct. Biol.* **2015,** *35*, 116-124.

(23) Zhu, W.; Liu, Y., Ring Contraction Catalyzed by the Metal-Dependent Radical SAM Enzyme: 7-Carboxy-7-deazaguanine Synthase from B. multivorans. Theoretical Insights into the Reaction Mechanism and the Influence of Metal Ions. *ACS Catal.* **2015,** *5* (7), 3953-3965.

(24) Griller, D.; Ingold, K. U., Free-radical clocks. *Acc. Chem. Res.* **1980,** *13* (9), 317-323.

(25) Newcomb, M.; Esala, R.; Chandrasena, P.; Lansakara-P, D. S. P.; Kim, H.-Y.; Lippard, S. J.; Beauvais, L. G.; Murray, L. J.; Izzo, V.; Hollenberg, P. F.; Coon, M. J., Desaturase Reactions Complicate the Use of Norcarane as a Mechanistic Probe. Unraveling the Mixture of Twenty-Plus Products Formed in Enzyme-Catalyzed Oxidations of Norcarane. *J. Org. Chem.* **2007,** *72* (4), 1121-1127.

(26) Valentine, A. M.; Le Tadic-Biadatti, M. H.; Toy, P. H.; Newcomb, M.; Lippard, S. J., Oxidation of ultrafast radical clock substrate probes by the soluble methane monooxygenase from Methylococcus capsulatus (Bath). *J. Biol. Chem.* **1999,** *274*, 10771-10776.

(27) Newcomb, M.; Le Tadic-Biadatti, M. H.; Chestney, D. L.; Roberts, E. S.; Hollenberg, P. F., A nonsynchronous concerted mechanism for cytochrome P-450 catalyzed hydroxylation. *J. Am. Chem. Soc.* **1995,** *117*, 12085-12091.

(28) Kemball, M. L.; Walton, J. C.; Ingold, K. U., The conformations of cycloalkylmethyl radicals and barriers to internal rotation. *J. Chem. Soc., Perkin Trans.* **1982,** *2*, 1017-1023.

(29) Smith, D. M.; Nicolaides, A.; Golding, B. T.; Radom, L., Ring opening of the cyclopropylcarbinyl radical and its N- and O- substituted analogues: A theoretical examination of very fast unimolecular reactions. *J. Am. Chem. Soc.* **1998,** *120* (39), 10223-10233.

(30) Datta, A.; Hrovat, D. A.; Borden, W. T., Calculations Predict Rapid Tunneling by Carbon from the Vibrational Ground State in the Ring Opening of Cyclopropylcarbinyl Radical at Cryogenic Temperatures. *J. Am. Chem. Soc.* **2008**, *130* (21), 6684-6685.

(31) Jäger, C. M.; Hennemann, M.; Clark, T., The Effect of a Complexed Lithium Cation on a Norcarane-Based Radical Clock. *Chem. Eur. J.* **2009,** *15* (10), 2425-2433.

(32) Jäger, C. M.; Hennemann, M.; Mieszała, A.; Clark, T., An ab initio and Density Functional Theory Study of Radical-Clock Reactions. *J. Org. Chem.* **2008,** *73* (4), 1536-1545.

(33) Hioe, J.; Savasci, G.; Brand, H.; Zipse, H., The Stability of Cα Peptide Radicals: Why Glycyl Radical Enzymes? *Chem. Eur. J.* **2011,** *17* (13), 3781-3789.

(34) Hioe, J.; Zipse, H., Radicals in enzymatic catalysis - A thermodynamic perspective. *Faraday Discuss.* **2010,** *145*, 301-313.

(35) Hioe, J.; Zipse, H., Radical stability and its role in synthesis and catalysis. *Org. Biomol. Chem.* **2010,** *8* (16), 3609-3617.

(36) Wood, G. P. F.; Gordon, M. S.; Radom, L.; Smith, D. M., Nature of Glycine and Its α-Carbon Radical in Aqueous Solution: A Theoretical Investigation. *J. Chem. Theory Comput.* **2008,** *4* (10), 1788-1794.

(37) Croft, A. K.; Easton, C. J.; Kociuba, K.; Radom, L., Strategic use of amino acid N-substituents to limit α-carbon- centered radical formation and consequent loss of stereochemical integrity. *Tetrahedron Asymmetry* **2003,** *14* (19), 2919-2926.

(38) Croft, A. K.; Easton, C. J.; Radom, L., Design of radical-resistant amino acid residues: A combined theoretical and experimental investigation. *J. Am. Chem. Soc.* **2003,** *125* (14), 4119-4124.

(39) Wood, G. P. F.; Moran, D.; Jacob, R.; Radom, L., Bond Dissociation Energies and Radical Stabilization Energies Associated with Model Peptide-Backbone Radicals. *J. Phys. Chem. A* **2005,** *109*, 6318-6325.

(40) Hioe, J.; Zipse, H., Hydrogen Transfer in SAM-Mediated Enzymatic Radical Reactions. *Chem. Eur. J.* **2012,** *18* (51), 16463-16472.

(41) Mardirossian, N.; Head-Gordon, M., How Accurate Are the Minnesota Density Functionals for Noncovalent Interactions, Isomerization Energies, Thermochemistry, and Barrier Heights Involving Molecules Composed of Main-Group Elements? *J. Chem. Theory Comput.* **2016,** *12* (9), 4303-4325.

(42) Peverati, R.; Truhlar, D. G., M11-L: A Local Density Functional That Provides Improved Accuracy for Electronic Structure

Calculations in Chemistry and Physics. *J. Phys. Chem. Lett.* **2012,** *3* (1), 117-124.

(43) Grimme, S.; Antony, J.; Ehrlich, S.; Krieg, H.; S., G.; J., A.; T., S.; C., M.-L., A consistent and accurate ab initio parametrization of density functional dispersion correction (DFT-D) for the 94 elements H-Pu. *J. Chem. Phys.* **2010,** *132* (15), 154104.

(44) Olsen, L.; Rydberg, P.; H. Rod, T. H.; Ryde, U., Prediction of Activation Energies for Hydrogen Abstraction by Cytochrome P450. *J. Med. Chem.* **2006**, 49 (22), 6489-6499.

(45) Shaik, S.; Kumar, D.; Visser, S. P., A Valence Bond Modeling of Trends in Hydrogen Abstraction Barriers and Transition States of Hydroxylation Reactions Catalyzed by Cytochrome P450 Enzymes. *J. Am. Chem. Soc.* **2008**, 130 (31), 10128-10140.

(46) Salomon-Ferrer, R.; Götz, A. W.; Poole, D.; Le Grand, S.; Walker, R. C., Routine Microsecond Molecular Dynamics Simulations with AMBER on GPUs. 2. Explicit Solvent Particle Mesh Ewald. *J. Chem. Theory Comput.* **2013,** *9* (9), 3878-3888.

(47) Le Grand, S.; Götz, A. W.; Walker, R. C., SPFP: Speed without compromise—A mixed precision model for GPU accelerated molecular dynamics simulations. *Comput. Phys. Commun.* **2013,** *184* (2), 374-380.

(48) Götz, A. W.; Williamson, M. J.; Xu, D.; Poole, D.; Le Grand, S.; Walker, R. C., Routine Microsecond Molecular Dynamics Simulations with AMBER on GPUs. 1. Generalized Born. *J. Chem. Theory Comput.* **2012,** *8* (5), 1542-1555.

(49) Case, D. A.; Botello-Smith, W. M.; Betz, R.M.; Cerutti, D. S.; Cheatham, III, T.E.; Darden, T.A.; Duke, R.E.; Giese, T.J.; Gohlke, H.; Goetz, A.W.; Homeyer, N.; Izadi, S.; Janowski, P.; Kaus, J.; Kovalenko, A.; Lee, T.S.; LeGrand, S.; Li, P.; Lin, C.; Luchko, T.; Luo, R.; Madej, B.; Mermelstein, D.; Merz, K.M.; Monard, G.; Nguyen, H.; Nguyen, H.T.; Omelyan, I.; Onufriev, A.; Roe, D.R.; Roitberg, A.; Sagui, C.; Simmerling, C.L.; Swails, J.; Walker, R.C.; Wang, J.; Wolf, R.M.; Wu, X.; Xiao, L.; and Kollman P.A., University of California, San Francisco, 2016.

(50) Saez, D. A.; Vöhringer-Martinez, E., A consistent S-Adenosylmethionine force field improved by dynamic Hirshfeld-I atomic charges for biomolecular simulation. *J. Comput. Aided Mol. Des.* **2015,** *29* (10), 951-961.

(51) Bame, J.; Hoeck, C.; Carrington, M. J.; Butts, C. P.; Jäger, C. M.; Croft, A. K., Improved NOE fitting for flexible molecules based on molecular mechanics data – a case study with S-adenosylmethionine. *Phys. Chem. Chem. Phys* **2018,** *20* (11), 7523-7531.

(52) Carvalho, A. T. P.; Swart, M., Electronic Structure Investigation and Parametrization of Biologically Relevant Iron–Sulfur Clusters. *J. Chem. Inf. Model.* **2014,** *54* (2), 613-620.

(53) Li, P.; Roberts, B. P.; Chakravorty, D. K.; Merz, K. M., Rational Design of Particle Mesh Ewald Compatible Lennard-Jones Parameters for +2 Metal Cations in Explicit Solvent. *J. Chem. Theory Comput.* **2013,** *9* (6), 2733-2748.

(54) Horinek, D.; Herz, A.; Vrbka, L.; Sedlmeier, F.; Mamatkulov, S. I.; Netz, R. R., Specific ion adsorption at the air/water interface: The role of hydrophobic solvation. *Chem. Phys. Lett.* **2009,** *479* (4), 173-183.

(55) Bayly, C. I.; Cieplak, P.; Cornell, W. D.; Kollman, P. A., A well-behaved electrostatic potential based method using charge restraints for deriving atomic charges – The RESP model. *J. Phys. Chem.* **1993,** *97* (40), 10269-10280.

(56) Goldman, P. J.; Grove, T. L.; Booker, S. J.; Drennan, C. L., X-ray analysis of butirosin biosynthetic enzyme BtrN redefines structural motifs for AdoMet radical chemistry. *Proc. Natl. Acad. Sci.* **2013,** *110* (40), 15949-15954.

(57) Umitsu, M.; Nishimasu, H.; Noma, A.; Suzuki, T.; Ishitani, R.; Nureki, O., Structural basis of AdoMet-dependent aminocarboxypropyl transfer reaction catalyzed by tRNA-wybutosine synthesizing enzyme, TYW2. *Proc. Natl. Acad. Sci.* **2009,** *106* (37), 15616-15621.

(58) Becke, A. D., Density-functional thermochemistry. III. The role of exact exchange. *J. Chem. Phys.* **1993,** *98*, 5648.

(59) Lee, C.; Yang, W.; Parr, R. G., Development of the Colle-Salvetti correlation-energy formula into a functional of the electron density. *Phys. Rev. B: Condens. Matter Mater. Phys.* **1988,** *37*, 785.

(60) Stephens, P. J.; Devlin, F. J.; Chabalowski, C. F.; Frisch, M. J., Ab Initio Calculation of Vibrational Absorption and Circular Dichroism Spectra Using Density Functional Force Fields. *J. Phys. Chem.* **1994,** *98*, 11623-11627.

(61) Ditchfield, R.; Hehre, W. J.; Pople, J. A., Self-Consistent Molecular-Orbital Methods. IX. An Extended Gaussian-Type Basis for Molecular-Orbital Studies of Organic Molecules. *J. Chem. Phys.* **1971,** *54* (2), 724-728.

(62) Dunning, T. H., Gaussian basis sets for use in correlated molecular calculations. I. The atoms boron through neon and hydrogen. *J. Chem. Phys.* **1989,** *90* (2), 1007-1023.

(63) Clark, T.; Chandrasekhar, J.; Spitznagel, G. W.; Schleyer, P. V. R., Efficient diffuse function-augmented basis sets for anion calculations. III. The 3-21+G basis set for first-row elements, Li–F. *J. Comput. Chem.* **1983,** *4* (3), 294-301.

(64) Tomasi, J.; Mennucci, B.; Cammi, R., Quantum mechanical continuum solvation models. *Chem. Rev.* **2005,** *105* (8), 2999-3093.

(65) Frisch, M. J.; Trucks, G. W.; Schlegel, H. B.; Scuseria, G. E.; Robb, M. A.; Cheeseman, J. R.; Scalmani, G.; Barone, V.; Mennucci, B.; Petersson, G. A.; Nakatsuji, H.; Li, X.; Caricato, M.; Marenich, A.; Bloino, J.; Janesko, B. G.; Gomperts, R.;, Hratchian, H. P.; Ortiz, J. V.; Izmaylov, A. F.; Sonnenberg, J. L.; Williams-Young, D.; Ding, F.; Lipparini, F.; Egidi, F.; Goings, J.; Peng, B.; Petrone, A.; Henderson, T.; Ranasinghe, D.; Zakrzewski, V. G.; Gao, J.; Rega, N.; Zheng, G.; Liang, W.; Hada, M.; Ehara, M.; Toyota, K.; Fukuda, R.; Hasegawa, J.; Ishida, M.; Nakajima, T.; Honda, Y.; Kitao, O.; Nakai, H.; Vreven, T.; Throssell, K.; Montgomery, J. A.; Jr., Peralta, J. E.; Ogliaro, F.; Bearpark, M.; Heyd, J. J.; Brothers, E.; Kudin, K. N.; Staroverov,V. N.; Keith, T.; Kobayashi, R.; Normand, J.; Raghavachari, K.; Rendell, A.; Burant, J. C.; Iyengar, S. S.; Tomasi, J;. Cossi, M.; Millam, J. M.; Klene, M.; Adamo, C.; Cammi, R.; Ochterski, J. W.; Martin, R. L.; Morokuma, K.; Farkas, O.; Foresman, J. B.; Fox D. J., *Gaussian 09*. 2009.

(66) Wang, J.; Wang, W.; Kollman, P. A.; Case, D. A., Automatic atom type and bond type perception in molecular mechanical calculations. *J. Mol. Graph. Model.* **2006,** *25* (2), 247-260.

(67) Berendsen, H. J. C.; Grigera, J. R.; Straatsma, T. P., The missing term in effective pair potentials. *J. Phys. Chem.* **1987,** *91* (24), 6269-6271.

(68) Gordon, J. C.; Myers, J. B.; Folta, T.; Shoja, V.; Heath, L. S.; Onufriev, A., H++: a server for estimating pKas and adding missing hydrogens to macromolecules. *Nucleic Acids Res.* **2005,** *33* (Web Server issue), W368-W371.

(69) Darden, T.; York, D.; Pedersen, L., Particle mesh Ewald: An N·log(N) method for Ewald sums in large systems. *J. Chem. Phys.* **1993,** *98* (12), 10089-10092.

(70) Stewart, J. J. P., MOPAC2009. Stewart Computational Chemistry: Colorado Springs, 2008.

(71) Stewart, J. J. P., Optimization of parameters for semiempirical methods VI: more modifications to the NDDO approximations and re-optimization of parameters. *J. Mol. Model.* **2013,** *19* (1), 1-32.

(72) Shao, Y.; Gan, Z.; Epifanovsky, E.; Gilbert, A. T. B.; Wormit, M.; Kussmann, J.; Lange, A. W.; Behn, A.; Feng, X.; Ghosh, D.; Goldey, M.; Horn, P. R.; Jacobson, L. D.; Kaliman, I.; Khaliullin, R. Z.; Kuś, T.; Liu, J.; Proynov, E. I.; Rhee, Y. M.; Richard, R. M.; Rohrdanz, A.; Steele, R. P.; Sundstrom,E. J.; Iii, H. L. W.; Zimmerman, M.; Zuev, D.; Albrecht, B.; Alguire, E.; Austin, B.; Beran, G. J. O.; Bernard, Y. A.; Berquist, E.; Brandhorst, B.; Bravaya, K.; Brown,S. T.; Casanova, D.; Chang, C.; Chien, S. H.; Closser, K. D.; Crittenden, D. L.; Distasio Jr, R. A.; Do, H.; Dutoi, A. D.; Edgar, G. Fatehi, S.; Fusti-molnar, L.; Ghysels, A.; Golubeva, A.; Gomes, J.; Hanson-heine, M. W. D.; Philipp, H. P.; Hauser, A. W.; Hohenstein, E. G.; Holden, Z. C.; Jagau, T.; Kaduk, H. Ji, B.; Khistyaev, K.; Kim, J.; Kim, J.; King, R. A.; Klunzinger, P.; Kosenkov, D.; Kowalczyk, T.; Krauter, C. M.; Lao, K. U.; Laurent, A. D.; Lawler, K. V.; Levchenko, V.; Lin, C. Y.; Liu, F.; Livshits, E.; Lochan, R. C.; Luenser, A.; Manohar,P.; Manzer, S. F.; Mao, S.; Marenich, A. V; Maurer,S. A.; Mayhall,N. J.; Neuscamman, E.; Oana, C. M.; Olivares-amaya, R.; Neill, P. O.; Parkhill, J. A.;

Perrine, T. M.; Peverati, R.; Rehn, D. R.; Rosta, E.; Russ, N. J.; Sharada, S. M.; Sharma, S.; Small, D. W.; Sodt, A.; Stein, T.; Stück, D.; Su,Y.; Thom, A. J. W.; Tsuchimochi, T.; Vanovschi, V.; Vydrov, O.; Wang, T.; Watson, M. A.; Wenzel, J.; White, A.; Williams, C. F.; Yang, J.; Yeganeh, S.; Yost, S. R.; Zhang, I. Y.; Zhang, X.; Zhao, Y.; Brooks, B. R.; Chan, K. L.; Chipman, D. M.; Cramer, C. J.; Goddard, W. A.; Gordon, M. S.; Hehre, W. J.; Klamt, A.; Iii, H. F. S.; Schmidt, M. W.; . Sherrill, C. D; Truhlar, D. G.; Warshel, A.; Xu, X.; Aspuru-guzik, A.; Baer, R.; Bell, A. T.; Besley, N. A.; Chai, D.; Dreuw, A.; Dunietz, B. D.; Furlani,T. R.; Steven, R.; Hsu, C.; Jung, Y.; Kong,J.; Lambrecht, D. S.; Liang, W.; Ochsenfeld, C.; Rassolov, V. A.; Lyudmila, V.; Subotnik, J. E.; Van Voorhis, T.; Herbert, J. M.; Anna, I.; Gill, M. Head-gordon, P. M. W.; Shao, Y.; Gan, Z.; Epifanovsky, E.; Gilbert, A. T. B., Advances in molecular quantum chemistry contained in the Q-Chem 4 program package. *Mol. Phys.* **2015,** *113* (2), 184-215.

(73) Boese, A. D.; Martin, J. M. L., Development of density functionals for thermochemical kinetics. *J. Chem. Phys.* **2004,** *121* (8), 3405-3416.

(74) Zhao, Y.; Truhlar, D. G., The M06 suite of density functionals for main group thermochemistry, thermochemical kinetics, noncovalent interactions, excited states, and transition elements: two new functionals and systematic testing of four M06-class functionals and 12 other functionals. *Theor. Chem. Acc.* **2008,** *120*, 215-241.

(75) Baboul, A. G.; Curtiss, L. A.; Redfern, P. C.; Raghavachari, K., Gaussian-3 theory using density functional geometries and zero-point energies. *The Journal of Chemical Physics* **1999,** *110* (16), 7650-7657.

(76) Friesner, R. A.; Banks, J. L.; Murphy, R. B.; Halgren, T. A.; Klicic, J. J.; Mainz, D. T.; Repasky, M. P.; Knoll, E. H.; Shelley, M.; Perry, J. K.; Shaw, D. E.; Francis, P.; Shenkin P.S., Glide: A New Approach for Rapid, Accurate Docking and Scoring. 1. Method and Assessment of Docking Accuracy. *J. Med. Chem.* **2004,** *47* (7), 1739-1749.

(77) Friesner, R. A.; Murphy, R. B.; Repasky, M. P.; Frye, L. L.; Greenwood, J. R.; Halgren, T. A.; Sanschagrin, P. C.; Mainz, D. T., Extra Precision Glide: Docking and Scoring Incorporating a Model of Hydrophobic Enclosure for Protein−Ligand Complexes. *J. Med. Chem.* **2006,** *49* (21), 6177-6196.

(78) Harder, E.; Damm, W.; Maple, J.; Wu, C.; Reboul, M.; Xiang, J. Y.; Wang, L.; Lupyan, D.; Dahlgren, M. K.; Knight, J. L.; Kaus, J. W.; Cerutti, D. S.; Krilov, G.; Jorgensen, W. L.; Abel, R.; Friesner, R. A., OPLS3: A Force Field Providing Broad Coverage of Drug-like Small Molecules and Proteins. *J. Chem. Theory Comput.* **2016,** *12* (1), 281-296.

Table of contents graphic:

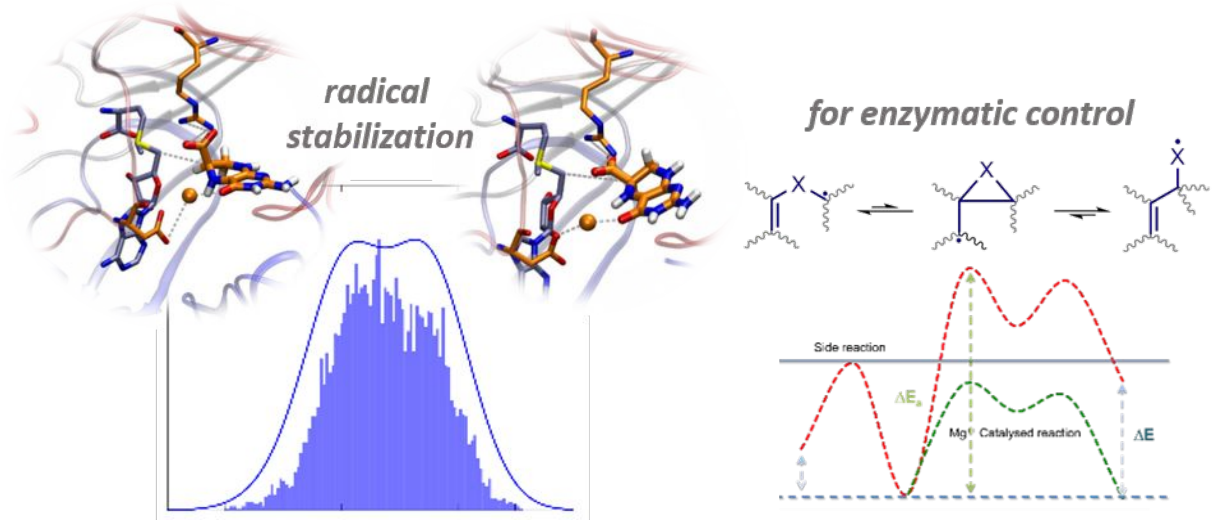

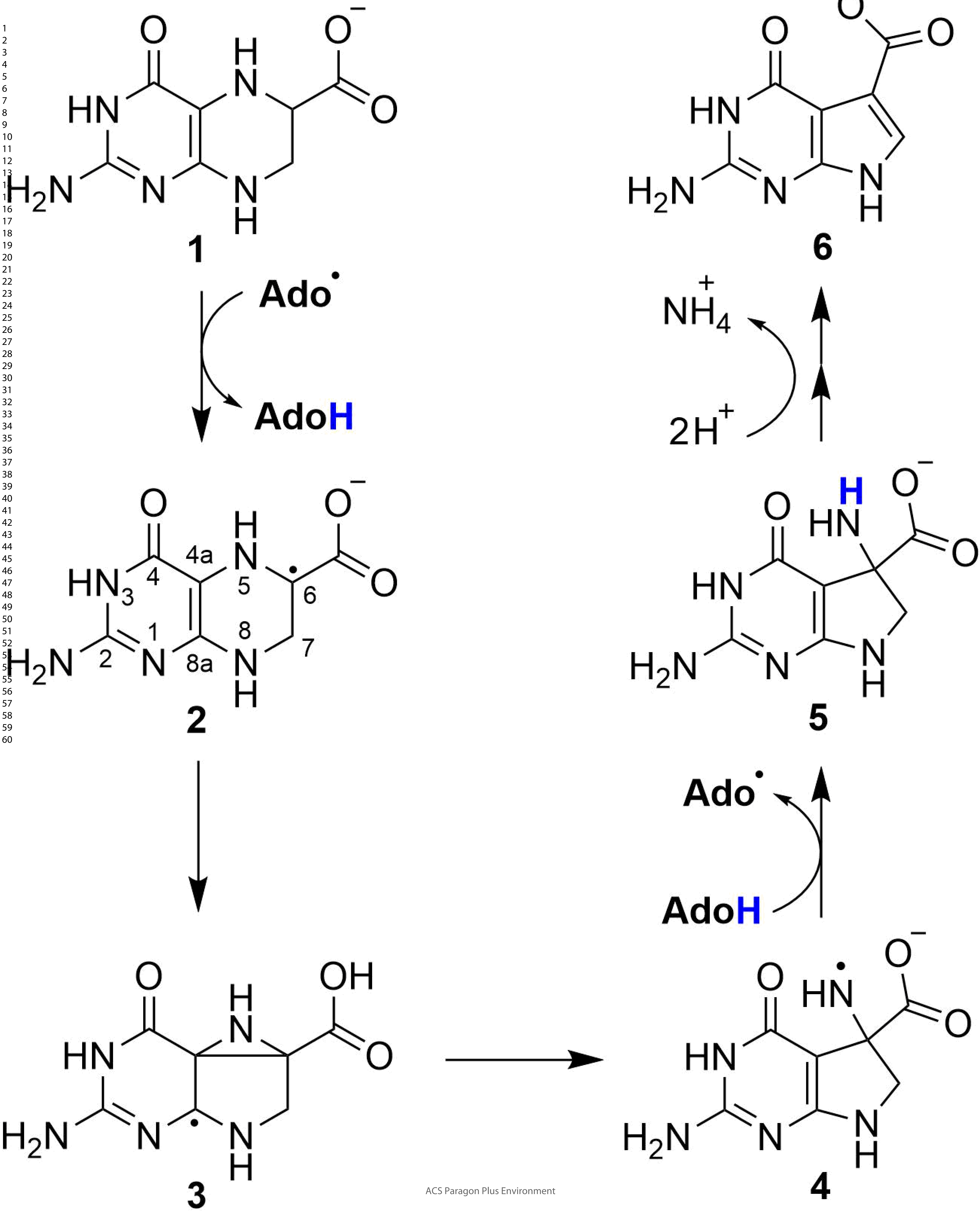
1
Ado•
AdoH
2
4a
4
HN3
5
6
1
8
7
2
8a
3
4
AdoH
Ado•
5
2H+
NH4+
6

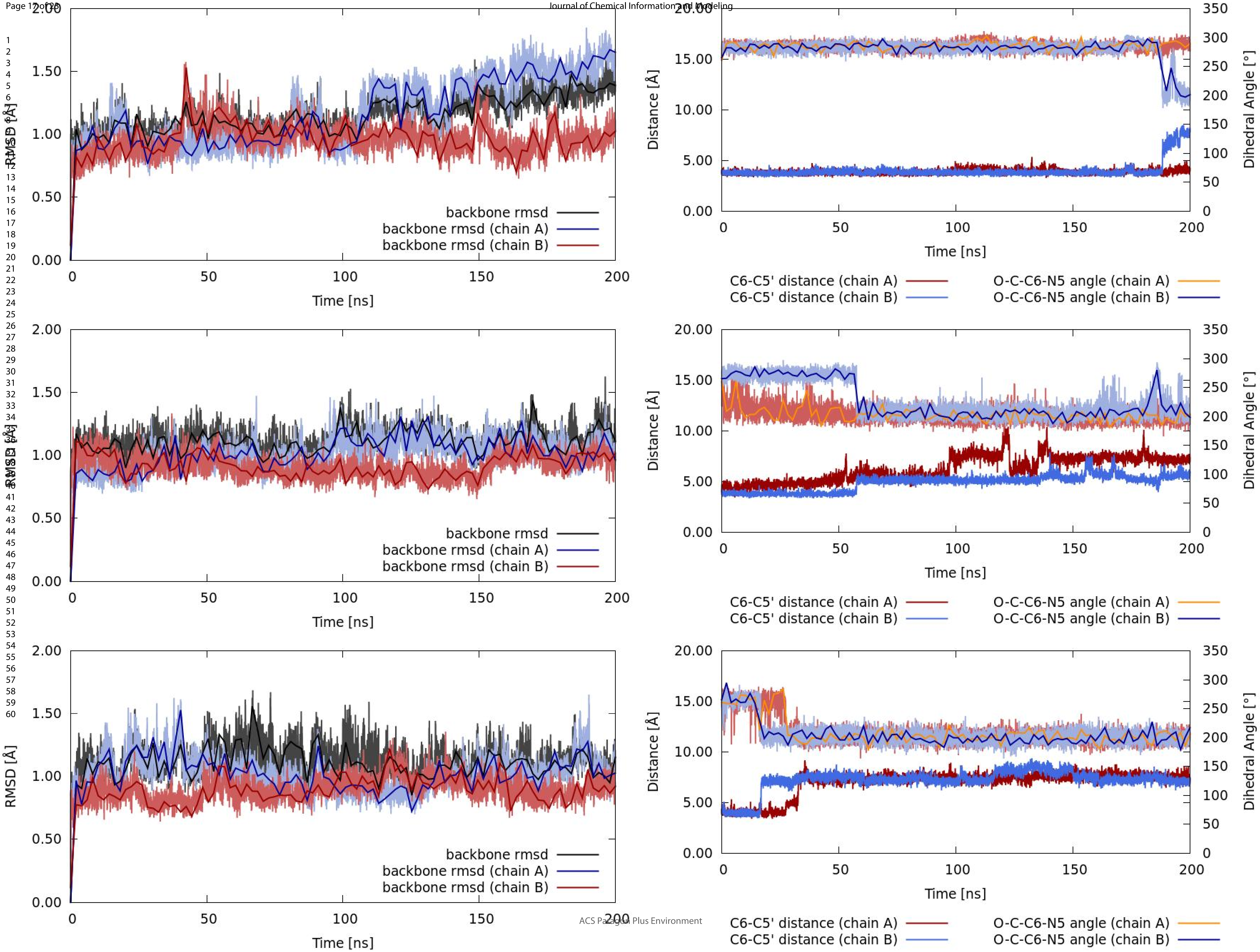
RMSD [Å]
2.00
1.50
1.00
0.50
0.00
0
50
100
150
200
Time [ns]
backbone rmsd
backbone rmsd (chain A)
backbone rmsd (chain B)
Distance [Å]
20.00
15.00
10.00
5.00
0.00
Dihedral Angle [°]
350
300
250
200
150
100
50
0
0
50
100
150
200
Time [ns]
C6-C5' distance (chain A)
C6-C5' distance (chain B)
O-C-C6-N5 angle (chain A)
O-C-C6-N5 angle (chain B)
RMSD [Å]
2.00
1.50
1.00
0.50
0.00
0
50
100
150
200
Time [ns]
backbone rmsd
backbone rmsd (chain A)
backbone rmsd (chain B)
Distance [Å]
20.00
15.00
10.00
5.00
0.00
Dihedral Angle [°]
350
300
250
200
150
100
50
0
0
50
100
150
200
Time [ns]
C6-C5' distance (chain A)
C6-C5' distance (chain B)
O-C-C6-N5 angle (chain A)
O-C-C6-N5 angle (chain B)
RMSD [Å]
2.00
1.50
1.00
0.50
0.00
0
50
100
150
200
Time [ns]
backbone rmsd
backbone rmsd (chain A)
backbone rmsd (chain B)
Distance [Å]
20.00
15.00
10.00
5.00
0.00
Dihedral Angle [°]
350
300
250
200
150
100
50
0
0
50
100
150
200
Time [ns]
C6-C5' distance (chain A)
C6-C5' distance (chain B)
O-C-C6-N5 angle (chain A)
O-C-C6-N5 angle (chain B)

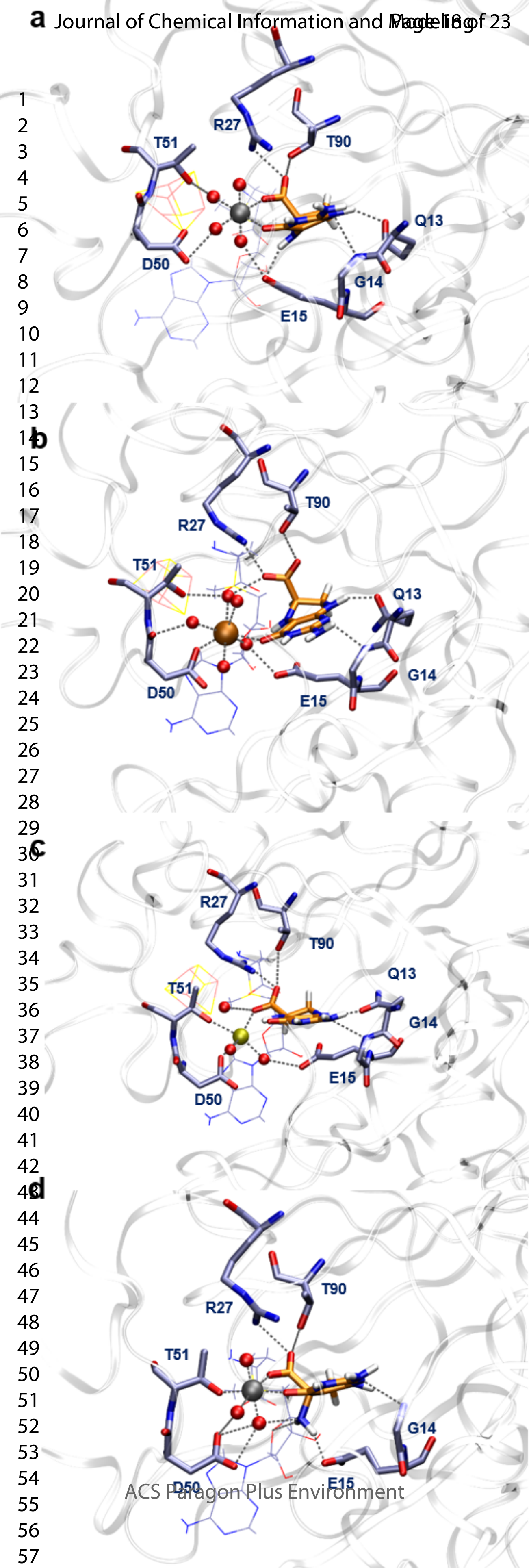
a
R27
T51
T90
Q13
D50
G14
E15
b
R27
T90
T51
Q13
G14
D50
E15
c
R27
T90
T51
Q13
G14
E15
D50
d
T90
R27
T51
G14
D50
E15

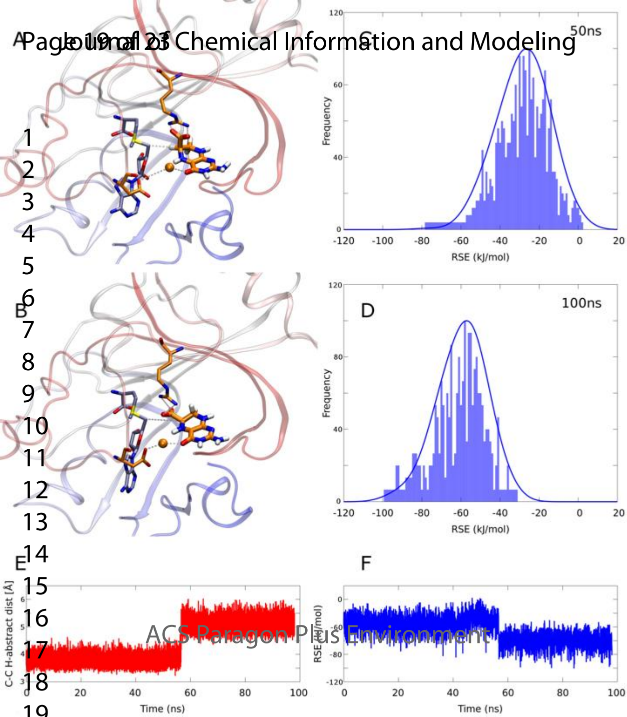
A
C
50ns
Frequency
0
40
60
120
-120
-100
-80
-60
-40
-20
0
20
RSE (kJ/mol)
B
D
100ns
Frequency
0
40
80
120
-120
-100
-80
-60
-40
-20
0
20
RSE (kJ/mol)
E
C-C H-abstract dist [Å]
3
4
5
6
0
20
40
60
80
100
Time (ns)
F
RSE (kJ/mol)
0
-60
-80
-120
0
20
40
60
80
100
Time (ns)

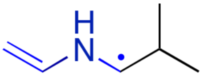

N1

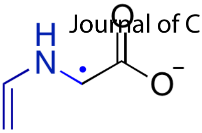

N2

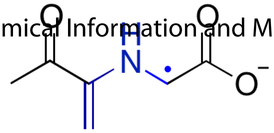

N3

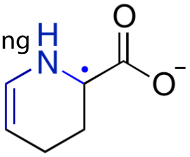

N4

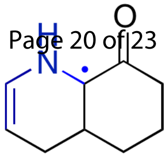

N5

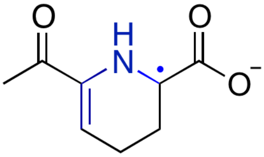

N6

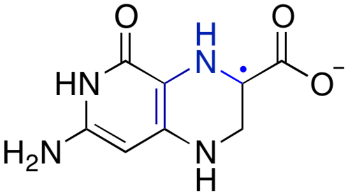

N7

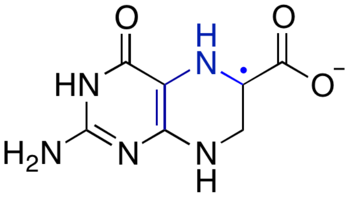

N8

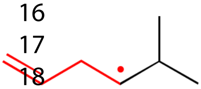

C1

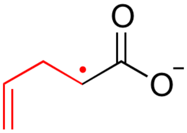

C2

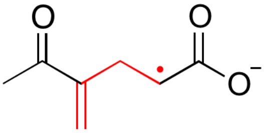

C3

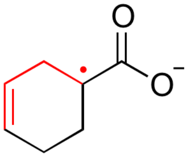

C4

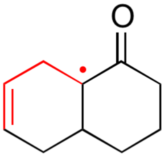

C5

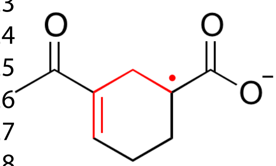

C6

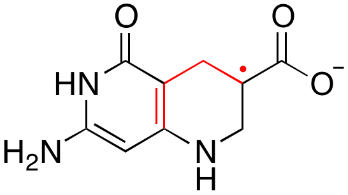

C7

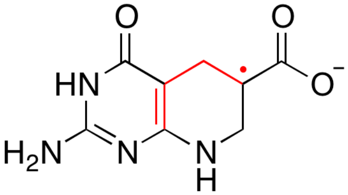

C8

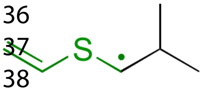

S1

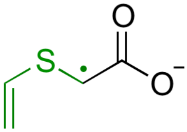

S2

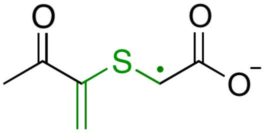

S3

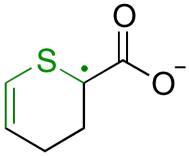

S4

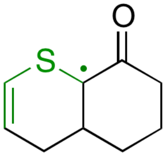

S5

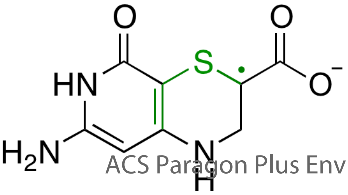

S7

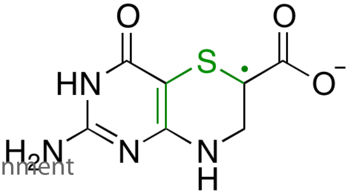

S8

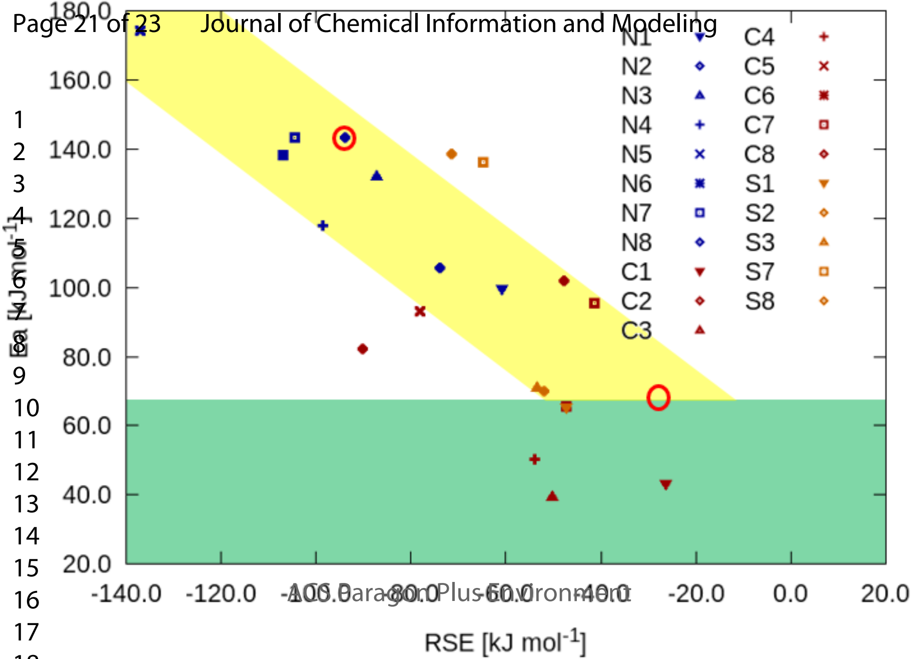
Ea [kJ mol^{-1}]
180.0
160.0
140.0
120.0
100.0
80.0
60.0
40.0
20.0
-140.0
-120.0
-100.0
-80.0
-60.0
-40.0
-20.0
0.0
20.0
RSE [kJ mol^{-1}]
N1
N2
N3
N4
N5
N6
N7
N8
C1
C2
C3
C4
C5
C6
C7
C8
S1
S2
S3
S7
S8

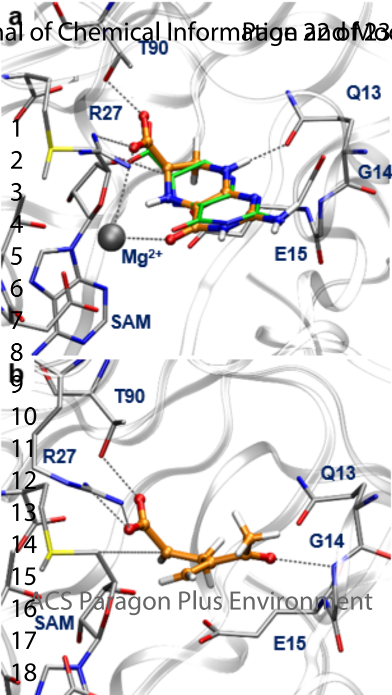
a
T90
Q13
R27
G14
Mg2+
E15
SAM
b
T90
R27
Q13
G14
SAM
E15

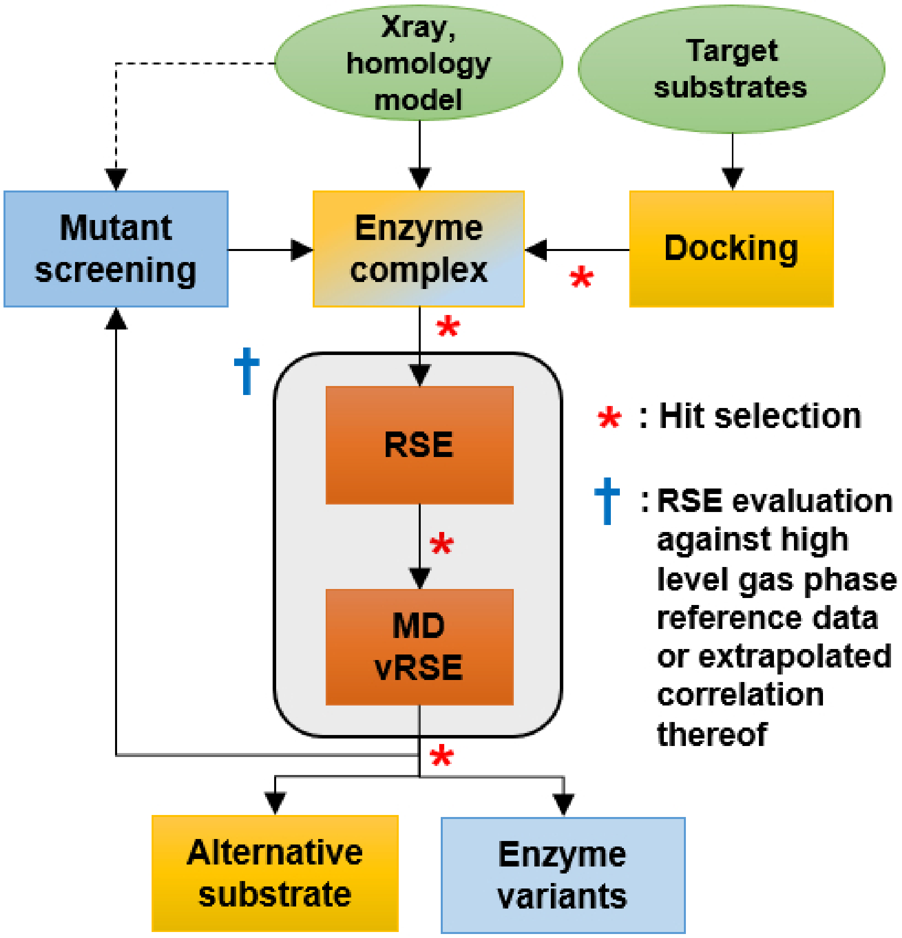
Xray, homology model
Target substrates
Mutant screening
Enzyme complex
Docking
*
*
†
RSE
*
MD vRSE
*
Alternative substrate
Enzyme variants
* : Hit selection
† : RSE evaluation against high level gas phase reference data or extrapolated correlation thereof

Figure 7. Proposed computational workflow for screening for alternative rSAM enzyme substrates and alternative mutants based on the rapid assessment of radical stabilization energies.

92x91mm (150 x 150 DPI)